Accepted Manuscript

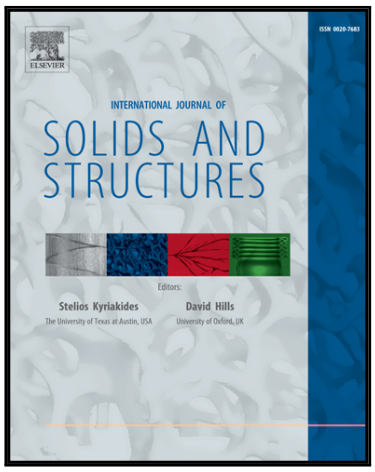

Influence of imperfect interface and fiber distribution on the antiplane effective magneto-electro-elastic properties for fiber reinforced composites

Y. Espinosa-Almeyda , H. Camacho-Montes , R. Rodríguez-Ramos , R. Guinovart-Díaz , J.C. López-Realpozo , J. Bravo-Castillero , F.J. Sabina

PII: S0020-7683(17)30015-X
DOI: 10.1016/j.ijsolstr.2017.01.016
Reference: SAS 9432

To appear in: *International Journal of Solids and Structures*

Received date: 2 June 2016
Revised date: 30 November 2016
Accepted date: 10 January 2017

Please cite this article as: Y. Espinosa-Almeyda , H. Camacho-Montes , R. Rodríguez-Ramos , R. Guinovart-Díaz , J.C. López-Realpozo , J. Bravo-Castillero , F.J. Sabina , Influence of imperfect interface and fiber distribution on the antiplane effective magneto-electro-elastic properties for fiber reinforced composites, *International Journal of Solids and Structures* (2017), doi: 10.1016/j.ijsolstr.2017.01.016

This is a PDF file of an unedited manuscript that has been accepted for publication. As a service to our customers we are providing this early version of the manuscript. The manuscript will undergo copyediting, typesetting, and review of the resulting proof before it is published in its final form. Please note that during the production process errors may be discovered which could affect the content, and all legal disclaimers that apply to the journal pertain.

ACCEPTED MANUSCRIPT

Highlights

- Asymptotic homogenization method provides accurate numerical result
- The spatial fiber distribution allows two composite property symmetry behavior
- The imperfect interphase has influence on the effective properties
- Magnetoelectric coupling is sensitive to fiber distribution and imperfection

ACCEPTED MANUSCRIPT

ACCEPTED MANUSCRIPT

Influence of imperfect interface and fiber distribution on the antiplane effective magneto-electro-elastic properties for fiber reinforced composites

Y. Espinosa-Almeyda[1], H. Camacho-Montes[1*], R. Rodríguez-Ramos[2], R. Guinovart-Díaz[2], J. C. López-Realpozo[2], J. Bravo-Castillero[2], F. J. Sabina[3].

[2]Instituto de Ingeniería y Tecnología, Universidad Autónoma de Ciudad Juárez, Av. Del Charro 450 Norte Cd. Juárez, Chihuahua. 32310, México.
yoanhealmeyda1209@gmail.com, hcamacho@uacj.mx

[1]Facultad de Matemática y Computación. Universidad de La Habana, San Lázaro y L, Vedado, La Habana, CP. 10400, Cuba.
reinaldo@matcom.uh.cu, guino@matcom.uh.cu, jclrealpozo@matcom.uh.cu, jbravo@matcom.uh.cu

[3]Instituto de Investigaciones en Matemáticas Aplicadas y en Sistemas, Universidad Nacional Autónoma de México, Apartado Postal 20-726, Delegación de Álvaro Obregón, 01000 México, D.F., México.
fjs@mym.iimas.unam.mx

*Corresponding author: H. Camacho-Montes[1], e-mail: hcamacho@uacj.mx

Keywords: Fiber-reinforced composites, effective properties, asymptotic homogenization method, magneto-electro-elastic coupling, imperfect contact conditions.

Abstract

The antiplane effective coefficients of two-phase piezoelectric-piezomagnetic periodic composite materials reinforced with cylindrical, unidirectional and periodically distributed fibers are computed by means of asymptotic homogenization method (AHM). The constituents have transversely isotropic properties belonging to 6mm symmetry group and the periodic distribution

ACCEPTED MANUSCRIPT

ACCEPTED MANUSCRIPT

of the fibers is assumed to be parallelogram-like as representative volume element (RVE). In the model, the imperfections are modeled as an idealization of spring-capacitor-inductor distributions at the interface. The antiplane local problems and the associated effective coefficients result of the AHM are explicitly described. The explicit formulae depend on the physical properties of the constituents of the phases and the constants that characterize the existence of the aforementioned imperfection. The validation of the present approach is shown by comparison with numerical results reported in the literature. The influences of the fiber spatial distributions and the imperfect fiber-matrix interface contact conditions on the effective properties are analyzed. Spatial fiber distribution induces some value changes in the magneto-electric coefficient and two possible composites property symmetry are obtained: monoclinic 2 and transversely isotropic. The effect of the imperfect contact parameter has a more pronounced value on the ME coefficient than the fiber distribution.

1. Introduction

Composite materials that exhibit either improved properties or new ones in comparison to their constituents have been the focus of the scientific community for many years to support modern technology. Considerable advantages, in some of them, have been the structure optimization, the physics properties manipulation and the emergence of new properties due to couplings, while preserving a comparable or improved functionality level (Li and Dunn, 1998).

The coupling magnetoelectric effect (ME) arises from cross or product properties, i.e., the polarization induced by a magnetic field, or conversely the magnetization induced by an electric field (Nan et al., 2008). The composites made of piezoelectric and piezomagnetic phases exhibit a coupling magnetoelectric effect, which does not exist in each phase, but appears as a result of the mechanical interaction between them. The coupling properties are important to design novel appropriate materials for smart device, broadband magnetic field probes, electromagnetic information transformation, sensors, actuation and controller, magnetoelectric memory cells (Wang, 2015; Xu and Xiao, 2015).

The pioneering works on magnetoelectric composites are reported by Van Suchtelen (1972), Van Run et al. (1974) and Van den Boomgaard et al. (1974). The magnetoelectric composites turn out to have higher magnetoelectric coefficient than single-phase materials, therefore many

ACCEPTED MANUSCRIPT

authors have focused their search on this line, e.g., Van den Boomgaard and Born (1978) and Bunget and Raetchi (1981) obtained magnetoelectric composites of the kind Ni - Zn ferrite - PZT and $BaTiO_3$ - Ni(Co, Mn)Fe_2O_4. The raise of dissimilar kinds of multi-phase composite materials (thin films (nanostructures), bulk, particulates, laminates, fibrous and others) is motivated by the interest in understanding the coupling phenomena for a better manipulation of effective properties (Harshe et al., 1993; Benveniste, 1995; Wu and Huang, 2000; Nan et al., 2008; Dinzart and Sabar 2011; Kuo, 2014; Wang et al., 2015 and Kuo and Huang, 2016).

The development of numerical models and experimental methods for materials characterization in different conditions is a field of research and development of strategic importance for the technology innovation. Micromechanics methods have been used to estimate the overall properties of periodic composites (see for instance the works of Eshelby, 1957; Mori and Tanaka, 1973; Mclaughlin, 1977; Benveniste, 1987, 1995; Hashin, 1990; Parton and Kudryavtsev, 1993; Nemat-Nasser and Hori, 1999; Aboudi, 2001; Tong et al., 2008; Kuo, 2011; Yan et al., 2013; Kuo and Chen, 2015). One of them, the asymptotic homogenization method (AHM), which is based on the double scale asymptotic expansion (see books of Pobedrya, 1984; Bakhvalov and Panasenko, 1989), is the tool, we applied in the present contribution. The AHM is an accurate mathematical tool that has been used in several works for effective properties estimation in elastic composites (López-Realpozo et al., 2014), piezoelectric composites (Rodríguez-Ramos et al., 2013), magneto-electro-elastic composites (Guinovart-Díaz et al., 2013) and thermo-magneto-electro-elastic composites (Sixto-Camacho et al., 2013), among others.

The prediction of the overall properties of magneto-electro-elastic (MEE) composites has aroused great interest among researchers, showing great impact on those composites where the coupled phenomena is induced from discontinuous reinforcements. The bonding condition at the interface between the fiber and matrix is one of the important factors for the analysis and control of the resulting material properties. The perfect bonding condition is an idealization that may be inadequate for the description of the physical nature and mechanical behavior of the interface region. The complicated description of the interface still motivates the necessity to introduce new simplified theoretical approaches. They simulate a more real behavior of the idealized composite and the way to include the caused effects on the interface during the conformation of the new composite (Wang and Pan, 2007; Wüerkner et al., 2013; Otero et al., 2014; Wang, 2015).

ACCEPTED MANUSCRIPT

In particular, the linear spring interface and the interphase models are frequently employed to simulate the interface regions in fiber-reinforced composites. Both models, in general, illustrates some interface damages or the thin glue layer between two adjacent phases. In the first, the existence of displacement and/or stress discontinuities on the interface is assumed and represented by linear and nonlinear laws (Hashin, 1991; Benveniste and Miloh, (2001); Wang et al., 2005, López-Realpozo et al., 2011; Sevostianov et al., 2012; Kuo and Huang, 2016). The second model (known as three-phase model) is described as an active region, considered as a thin layer (interphase or mesophase) between the fiber and matrix (Hashin, 2002; Dinzart and Sabar, 2011; Sevostianov et al., 2012; Yan et al., 2013). The last representation is a real and excellent approximation for the complex phenomenon that may occurs in the fiber-matrix transition zone. It is conveniently used in analytical or numerical solutions of boundary-value problems of composite materials Wang et al. (2005).

In this work, the formal description reported by Wang and Pan (2007), Rodríguez-Ramos et al., (2010) for the interface models is further continued. Here, the existence of mechanic, electric and magnetic imperfections at the interface between piezoelectric and piezomagnetic phases are considered. Furthermore, the influence of the imperfect contact in the whole set of MEE effective properties of fiber unidirectional reinforced composite with parallelogram-like RVE is further studied. The AHM is applied to the heterogeneous media and techniques of the complex variable are applied to solve the local problems derived by the homogenization procedure. Brief formulation of the antiplane local problems, the solution of the local problems and the derivation of the effective coefficients are given.

The main contribution of the present work is focused on the effect of the spatial fiber distribution and the effect of the mechanical, electrical and magnetical imperfect contact conditions on the magneto-electric (ME) effective coefficient. This effect has been only previously reported for hexagonal and square unit cell (Espinosa-Almeyda et al., 2011). Then, a wider range of parallelogram-like RVEs is studied, which is given as consequence of the several cases of fiber distributions considered herein. As a result of fiber distribution, it is possible to obtain two classes of symmetry point groups (monoclinic 2 and transversely isotropic structures) for global behavior and other ME effective properties are arisen for these types of symmetries. For some cases, higher ME moduli than previously reported ones can be achieved. In addition,

ACCEPTED MANUSCRIPT

the effects of the imperfect contact condition at the interphase, the fiber volume fraction, and the selection of the constituent phases on the antiplane effective properties are discussed.

2. Heterogeneous problem formulation and basic formulation

The composite is defined $\Omega \subset \mathrm{R}^3$ in the Cartesian system of coordinates (x_1, x_2, x_3) with origin O as can be seen in Fig.1 (a). This region Ω represents a solid material which responds to the linear coupling among the anti-plane shear and the inplane (Ox_1x_2) electric and magnetic fields. The composite geometric description is characterized by a two-phase reinforced structure (fiber/matrix) in which the fiber distribution is represented by a parallelogram-like array. The unidirectional, circular, identical and continuous fibers are embedded in a medium (matrix) (Fig. 1(a)). They are periodically distributed without overlapping and infinitely long in the Ox_3 direction.

The piezoelectric and piezomagnetic homogeneous constituents have transversely isotropic properties and belong to the crystal symmetry punctual group $6mm$. The Ox_3 axis for both the fiber and the matrix is parallel to the fiber direction. The materials properties satisfy the conditions of symmetry $C_{ijkl} = C_{jikl} = C_{ijlk} = C_{klij}$, $e_{kij} = e_{kji}$, $q_{kij} = q_{kji}$, $\kappa_{ik} = \kappa_{ki}$, $\alpha_{ik} = \alpha_{ki}$ and $\mu_{ik} = \mu_{ki}$, and the positivity $\exists\ m_1 > 0,\ \forall\ A \in \mathbb{E}_s^3,\ C_{ijkl}(\mathbf{x}/\varepsilon)A_{ij}A_{kl} \geq m_1 A_{ij}A_{kl}$, $\exists\ m_2 > 0,\ \forall \mathbf{a} \in \mathbb{R}^3,\ \kappa_{ik}(\mathbf{x}/\varepsilon)a_i a_k \geq m_2 a_i a_k$ and $\exists\ m_3 > 0,\ \forall \mathbf{b} \in \mathbb{R}^3,\ \mu_{ik}(\mathbf{x}/\varepsilon)b_i b_k \geq m_3 b_i b_k$, where m_1, m_2 and m_3 are positive constants, and $\mathbb{E}_s^3$ is the space of symmetric 3×3 matrices. Also, for the piezoelectric (piezomagnetic) constituents the piezomagnetic (piezoelectric) properties have null values, and both constituents have null magnetoelectric properties.

The associated structure of the composite in the normal plane Ox_1x_2 to cylindrical axis for the RVE at the microscale level is showed in Fig. 1(b) and it is characterized in the local Cartesian system of coordinates $\{O; y_1, y_2, y_3\}$. Here, the appropriate RVE denoted as Y is taken as parallelograms whose fiber cross section is a circle of radius R_0 in the Oy_1y_2-plane. The regions occupied by the matrix $S_1\ (\gamma = 1)$ and the fiber $S_2\ (\gamma = 2)$ interact throughout the circular interphase denoted by $\Gamma = \left\{z : z = R_0 e^{i\theta}, 0 \leq \theta \leq 2\pi\right\}$ such as, $\mathrm{Y} = S_1 \cup S_2$ and

ACCEPTED MANUSCRIPT

$S_1 \cap S_2 = \varnothing$. Furthermore, the RVE is considered to have periodicity property on the complex plane $z = y_1 + i y_2$ where ω_1 and ω_2 are the principal periods and θ_1 the angle of inclination of the cell, see Fig. 1(b). The percolation fiber volume fraction for $\theta_1 = 30^0$, 40^0, 50^0, 60^0, 70^0, 80^0 and 90^0 are equal to 0.421, 0.571, 0.650, 0.732, 0.906, 0.835, 0.813, 0.797, and 0.785 respectively.

The antiplane constitutive equations for the magneto-electro-elastic materials under the previous description can be written (following the formulation of Nan, 1994; Li and Dunn, 1998) by components in the forms

$$\sigma_{\beta 3} = 2C_{1313}\varepsilon_{\beta 3} - e_{113}E_\beta - q_{113}H_\beta, \tag{1}$$

$$D_\beta = 2e_{113}\varepsilon_{\beta 3} + \kappa_{11}E_\beta + \alpha_{11}H_\beta, \tag{2}$$

$$B_\beta = q_{113}\varepsilon_{\beta 3} + \alpha_{11}E_\beta + \mu_{11}H_\beta, \tag{3}$$

Being $\beta = 1, 2$. Here, $\sigma_{\beta 3}$ and $\varepsilon_{\beta 3}$ are the antiplane shear stress and strain, E_β and D_β are the inplane electric field and electric displacement components and, H_β and B_β are the inplane magnetic field and magnetic induction components. C_{1313}, e_{113}, q_{113}, α_{11}, κ_{11} and μ_{11} are the shear modulus, piezoelectric, piezomagnetic, magnetoelectric coupling, the dielectric permittivity and the magnetic permeability coefficients, respectively.

The equations associated to the theory of plane strain linear elasticity and the quasi-static approximation of the Maxwell's theory takes the form

$$\varepsilon_{\beta 3} = u_{3,\beta}/2, \tag{4}$$

$$E_\beta = -\partial\phi/\partial x_\beta = -\phi_{,\beta}, \tag{5}$$

$$H_\beta = -\partial\psi/\partial x_\beta = -\psi_{,\beta}, \tag{6}$$

where u_3 is the only non-null antiplane mechanical displacement and, ϕ and ψ are the respective electric and magnetic potentials implicated. The comma notation is used to represent the partial derivate relative to the x_β component, i.e., $(\bullet)_{,\beta} \equiv \partial(\bullet)/\partial x_\beta$.

The governing equations for a MEE composite Ω, in the static case and in absences of body forces, electric charges and electric current densities, take the form:

$$\sigma_{ij,j}=0,\ D_{i,i}=0,\ B_{i,i}=0. \tag{7}$$

Then, if Eqs. (7) are combined with Eqs. (1) – (6), it yields to the coupled system of partial differential equations with rapidly oscillating coefficients on Ω,

$$\begin{aligned}&(C_{1313}(\mathbf{y})\,u_{3,\beta}+e_{113}(\mathbf{y})\,\phi_{,\beta}+q_{113}(\mathbf{y})\,\psi_{,\beta})_{,\beta}=0,\\&(e_{113}(\mathbf{y})\,u_{3,\beta}-\kappa_{11}(\mathbf{y})\,\phi_{,\beta}-\alpha_{11}(\mathbf{y})\,\psi_{,\beta})_{,\beta}=0,\\&(q_{113}(\mathbf{y})\,u_{3,\beta}-\alpha_{11}(\mathbf{y})\,\phi_{,\beta}-\mu_{11}(\mathbf{y})\,\psi_{,\beta})_{,\beta}=0,\end{aligned} \tag{8}$$

$$u_3\big|_{\partial\Omega}=g_1(x),\ \phi\big|_{\partial\Omega}=g_2(x),\ \psi\big|_{\partial\Omega}=g_3(x) \tag{9}$$

The Eqs. (8) together with the boundary conditions, Eq. (9), represent the antiplane problems associated with the theory of the linear magneto-electro-elasticity for a heterogeneous structure Ω, where $g_1(x)$, $g_2(x)$ and $g_3(x)$ are infinitely differentiable functions on Ω.

The imperfections at the interphase are modeled as an idealization of the spring-capacitor-inductor layer model. They are measured as parameter functions of imperfections like linear spring $\hat{K}$, electrical capacitance $\hat{M}$ and magnetic inductance $\hat{N}$ according to Otero et al. (2014). They are characterized as follows:

$$[[\sigma_{\beta 3}^{(\gamma)}n_\beta^{(\gamma)}]]=0,\ [[D_\beta^{(\gamma)}n_\beta^{(\gamma)}]]=0,\ [[B_\beta^{(\gamma)}n_\beta^{(\gamma)}]]=0, \quad \text{on } \Gamma \tag{10}$$

$$\sigma_{\beta 3}^{(\gamma)}n_\beta^{(\gamma)}=(-1)^{\gamma+1}\hat{K}[[u_3]],\ D_\beta^{(\gamma)}n_\beta^{(\gamma)}=(-1)^{\gamma}\hat{M}[[\phi]],\ B_\beta^{(\gamma)}n_\beta^{(\gamma)}=(-1)^{\gamma}\hat{N}[[\psi]], \quad \text{on } \Gamma \tag{11}$$

In Eqs. (10) and (11), the normal component of the mechanical traction, electric displacement and magnetic flux are continuous across the interface Γ. They are proportional to the jump of mechanical displacements, electric and magnetic static potentials respectively (Wang and Pan, 2007). The combination of the positive values of $\hat{K}$, $\hat{M}$ and $\hat{N}$ parameters identify all possible imperfections existing between the idealized perfect contact case $\hat{K},\hat{M},\hat{N}\to\infty$ and the complete decoupled case $\hat{K}=\hat{M}=\hat{N}=0$ between the fiber and matrix. $n_\beta^{(\gamma)}$ is the $\beta-$component of the outward normal to the surface S_γ on Γ. $[[f^{(\gamma)}]]=f^{(1)}-f^{(2)}$ describes the jump of the function f across the interface taken from S_1 to S_2. It is possible to define dimensionless imperfect parameters as follow: $\hat{K}=\tilde{K}C_{1313}^{(1)}/R_0$, $\hat{M}=\tilde{M}\kappa_{11}^{(1)}/R_0$, and $\hat{N}=\tilde{N}\mu_{11}^{(1)}/R_0$. For numerical calculations, it is more convenient to propose that $K=1/\tilde{K}$, $M=-1/\tilde{M}$ and $N=-1/\tilde{N}$. Then, from now on for the imperfect parameters, we have: the

ACCEPTED MANUSCRIPT

ACCEPTED MANUSCRIPT

perfect limit case is $K = M = N = 0$ and the total decoupled is $K, M, N \to \infty$ between the fiber and matrix.

3. Asymptotic homogenization method: effective properties and antiplane local problems

The two scale asymptotic homogenization method is the tool used in this work. One scale, denoted by $\mathbf{y} = (y_1, y_2, y_3)$ characterizes the heterogeneities at microscopic or local level and other one, $\mathbf{x} = (x_1, x_2, x_3)$, describes the macroscopic or global behavior of the composite. The scales are related by $\mathbf{y} = \mathbf{x}/\varepsilon$, where the dimensionless parameter $\varepsilon = l/L$ ($\varepsilon << 1$) represents the ratio between the characteristic longitudes of the RVE (l) and the linear dimension of the composite (L), see Fig. 1. Fundamentally, the study for MEE fiber composites is derivated following the ideas of Pobedria (1984) and Bakhvalov and Panasenko (1989).

The desired solution for the statement of the problem Eqs. (8) – (11) should be searched by a set of interconnected problems, starting by the expansion of functions $\mathbf{U}$ that are infinitely differentiable and $Y-$periodic with respect to the local variable $\mathbf{y}$ and are represented by means of the two scale asymptotic expression

$$\mathbf{U}(\mathbf{x}) = \mathbf{U}^{(0)}(\mathbf{x}, \mathbf{y}) + \varepsilon \mathbf{U}^{(1)}(\mathbf{x}, \mathbf{y}) + \mathrm{O}(\varepsilon^2), \tag{12}$$

where $\mathbf{U}^{(1)} = (u_3^{(1)}, \phi^{(1)}, \psi^{(1)})^{\mathrm{T}}$ is the correction of the original function $\mathbf{U} = (u_3, \phi, \psi)^{\mathrm{T}}$ which are explicit functions of the so called local functions. These local functions are solutions of the well-known local (or canonical) problems that satisfy the resultant differential equations linked with the original problem in the RVE (Sixto-Camacho et al., 2013).

3.1 *Antiplane local problems formulation and effective properties*

The corresponding antiplane local problems, denoted as ${}_{13}\mathcal{L}$, ${}_{23}\mathcal{L}$, ${}_{1}\mathcal{I}$, ${}_{2}\mathcal{I}$, ${}_{1}\mathcal{P}$ and ${}_{2}\mathcal{P}$, are now formulated. The fundamental problem consists in finding the matching local functions $\mathbf{X}^{(\gamma)}$, $\mathbf{Y}^{(\gamma)}$ and $\mathbf{Z}^{(\gamma)}$ that satisfies the Laplace equations, the imperfect contact conditions at the interface Γ over the RVE. These conditions can be written as:

ACCEPTED MANUSCRIPT

$$
\begin{aligned}
&C_{1313}^{(\gamma)}\,\mathbf{X}_{,\beta\beta}^{(\gamma)}+e_{113}^{(\gamma)}\,\mathbf{Y}_{,\beta\beta}^{(\gamma)}+q_{113}^{(\gamma)}\,\mathbf{Z}_{,\beta\beta}^{(\gamma)}=0,\\
&e_{113}^{(\gamma)}\,\mathbf{X}_{,\beta\beta}^{(\gamma)}-\kappa_{11}^{(\gamma)}\,\mathbf{Y}_{,\beta\beta}^{(\gamma)}-\alpha_{11}^{(\gamma)}\,\mathbf{Z}_{,\beta\beta}^{(\gamma)}=0, \qquad \text{in } S_\gamma \ \ (\gamma=1,2) \qquad (13)\\
&q_{113}^{(\gamma)}\,\mathbf{X}_{,\beta\beta}^{(\gamma)}-\alpha_{11}^{(\gamma)}\,\mathbf{Y}_{,\beta\beta}^{(\gamma)}-\mu_{11}^{(\gamma)}\,\mathbf{Z}_{,\beta\beta}^{(\gamma)}=0,
\end{aligned}
$$

$$
\begin{aligned}
&\left(C_{1313}^{(\gamma)}\,\mathbf{X}_{,\beta}^{(\gamma)}+e_{113}^{(\gamma)}\,\mathbf{Y}_{,\beta}^{(\gamma)}+q_{113}^{(\gamma)}\,\mathbf{Z}_{,\beta}^{(\gamma)}\right)n_\beta^{(\gamma)}+\Phi_1\left(n_1^{(\gamma)}\delta_{1\lambda}+n_2^{(\gamma)}\delta_{2\lambda}\right)=\frac{(-1)^{\gamma+1}\tilde{K}C_{1313}^{(1)}}{R_0}[[\mathbf{X}]],\\
&\left(e_{113}^{(\gamma)}\,\mathbf{X}_{,\beta}^{(\gamma)}-\kappa_{11}^{(\gamma)}\,\mathbf{Y}_{,\beta}^{(\gamma)}-\alpha_{11}^{(\gamma)}\,\mathbf{Z}_{,\beta}^{(\gamma)}\right)n_\beta^{(\gamma)}+\Phi_2\left(n_1^{(\gamma)}\delta_{1\lambda}+n_2^{(\gamma)}\delta_{2\lambda}\right)=\frac{(-1)^{\gamma+1}\tilde{M}\kappa_{11}^{(1)}}{R_0}[[\mathbf{Y}]], \quad \text{on } \Gamma \qquad (14)\\
&\left(q_{113}^{(\gamma)}\,\mathbf{X}_{,\beta}^{(\gamma)}-\alpha_{11}^{(\gamma)}\,\mathbf{Y}_{,\beta}^{(\gamma)}-\mu_{11}^{(\gamma)}\,\mathbf{Z}_{,\beta}^{(\gamma)}\right)n_\beta^{(\gamma)}+\Phi_3\left(n_1^{(\gamma)}\delta_{1\lambda}+n_2^{(\gamma)}\delta_{2\lambda}\right)=\frac{(-1)^{\gamma+1}\tilde{N}\mu_{11}^{(1)}}{R_0}[[\mathbf{Z}]].
\end{aligned}
$$

To guarantee that the solution of the antiplane local problems is unique, the local functions should satisfy the null average condition $\langle\mathbf{X}\rangle=0$, $\langle\mathbf{Y}\rangle=0$ and $\langle\mathbf{Z}\rangle=0$, where $\langle f\rangle$ symbol identifies the volume average per unit length over Y, defined by $\langle f\rangle=|\mathrm{Y}|^{-1}\int_{\mathrm{Y}} f(\mathbf{y})d\mathbf{y}$. Also, $\delta_{1\lambda}$ and $\delta_{2\lambda}$ denote the Kronecker's delta functions where $\lambda=1$ is for the local problems ${}_{13}\boldsymbol{\mathcal{L}}$, ${}_{1}\boldsymbol{\mathcal{I}}$, and ${}_{1}\boldsymbol{\mathcal{P}}$, and $\lambda=2$, for the local problems ${}_{23}\boldsymbol{\mathcal{L}}$, ${}_{2}\boldsymbol{\mathcal{I}}$, and ${}_{2}\boldsymbol{\mathcal{P}}$. Here, the local functions $\mathbf{X}$, $\mathbf{Y}$, and $\mathbf{Z}$ represent the vector of displacement, the electrical and magnetic potential respectively over the RVE, and they are associated with the different local problems. These variables for each local problem are summarized in the following Table 1.

Table 1

The complete moduli of non-null effective coefficients for MEE composites associated with the antiplane local problems, with transversely isotropic piezoelectric and piezomagnetic constituents of 6*mm* symmetry, are compiled in the effective matrix

$$
\begin{pmatrix}\sigma_{23}\\ \sigma_{13}\\ D_1\\ D_2\\ B_1\\ B_2\end{pmatrix}=
\begin{array}{c}
\begin{matrix}{}_{23}\boldsymbol{\mathcal{L}} & {}_{13}\boldsymbol{\mathcal{L}} & {}_{1}\boldsymbol{\mathcal{I}} & {}_{2}\boldsymbol{\mathcal{I}} & {}_{1}\boldsymbol{\mathcal{P}} & {}_{2}\boldsymbol{\mathcal{P}}\end{matrix}\\
\begin{pmatrix}
C_{2323}^{*} & \boldsymbol{C_{2313}^{*}} & \boldsymbol{e_{132}^{*}} & e_{232}^{*} & \boldsymbol{q_{132}^{*}} & q_{232}^{*}\\
\boldsymbol{C_{1323}^{*}} & C_{1313}^{*} & e_{131}^{*} & \boldsymbol{e_{231}^{*}} & q_{131}^{*} & \boldsymbol{q_{231}^{*}}\\
\boldsymbol{e_{123}^{*}} & e_{113}^{*} & \kappa_{11}^{*} & \boldsymbol{\kappa_{12}^{*}} & \alpha_{11}^{*} & \boldsymbol{\alpha_{12}^{*}}\\
e_{223}^{*} & \boldsymbol{e_{213}^{*}} & \boldsymbol{\kappa_{21}^{*}} & \kappa_{22}^{*} & \boldsymbol{\alpha_{21}^{*}} & \alpha_{22}^{*}\\
\boldsymbol{q_{123}^{*}} & q_{113}^{*} & \alpha_{11}^{*} & \boldsymbol{\alpha_{12}^{*}} & \mu_{11}^{*} & \boldsymbol{\mu_{12}^{*}}\\
q_{223}^{*} & \boldsymbol{q_{213}^{*}} & \boldsymbol{\alpha_{21}^{*}} & \alpha_{22}^{*} & \boldsymbol{\mu_{21}^{*}} & \mu_{22}^{*}
\end{pmatrix}
\end{array}
\begin{pmatrix}\varepsilon_{23}\\ \varepsilon_{13}\\ E_1\\ E_2\\ H_1\\ H_2\end{pmatrix}. \qquad (15)
$$

ACCEPTED MANUSCRIPT

The antiplane effective properties are functions of the corresponding local problem solutions on the RVE, of the constituent properties, and of the geometrical characteristic of the composite. It is important to note that, the parallelogram-like periodic cell allows a better manipulation for the composite macroscopic properties. In this sense, the new composites may have a monoclinic 2 structure at a macroscopic level as result of the fiber distribution and that the composite is made of two transversely isotropic phases. Hence, it is possible to observe an increase in the number of effective coefficients (indicated in boldface in Eq. (15)) in comparison to the cases when the fibers have hexagonal or square distributions (for that case, the indicated boldface coefficients are null).

3.2 *Solutions of the antiplane local problems*

The solution for all antiplane local problems is determined by means of the methods of complex potential theory. The harmonic and doubly periodic local functions defined over the RVE, for each antiplane local problem (Eq. (14)), are found by means of the Laurent expansions of harmonic functions for the matrix and power expansions for the fiber, as follows

$$\mathbf{X}^{(1)}(z)=\mathrm{Re}\left\{\frac{a_0 z}{R_0}+\sum_{p=1}^{\infty}{}^{o}a_p\frac{R_0^p}{z^p}+\sum_{p=1}^{\infty}{}^{o}\sum_{k=1}^{\infty}{}^{o}a_k\sqrt{\frac{k}{p}}\,w_{kp}\frac{z^p}{R_0^p}\right\}=\mathrm{Re}\left\{\frac{a_0 z}{R_0}+\sum_{k=1}^{\infty}{}^{o}a_k R_0^k\frac{\zeta^{(k-1)}(z)}{(k-1)!}\right\},$$

$$\mathbf{Y}^{(1)}(z)=\mathrm{Re}\left\{\frac{b_0 z}{R_0}+\sum_{p=1}^{\infty}{}^{o}b_p\frac{R_0^p}{z^p}+\sum_{p=1}^{\infty}{}^{o}\sum_{k=1}^{\infty}{}^{o}b_k\sqrt{\frac{k}{p}}\,w_{kp}\frac{z^p}{R_0^p}\right\}=\mathrm{Re}\left\{\frac{b_0 z}{R_0}+\sum_{k=1}^{\infty}{}^{o}b_k R_0^k\frac{\zeta^{(k-1)}(z)}{(k-1)!}\right\},\quad \text{in } S_1 \quad (16)$$

$$\mathbf{Z}^{(1)}(z)=\mathrm{Re}\left\{\frac{e_0 z}{R_0}+\sum_{p=1}^{\infty}{}^{o}e_p\frac{R_0^p}{z^p}+\sum_{p=1}^{\infty}{}^{o}\sum_{k=1}^{\infty}{}^{o}e_k\sqrt{\frac{k}{p}}\,w_{kp}\frac{z^p}{R_0^p}\right\}=\mathrm{Re}\left\{\frac{e_0 z}{R_0}+\sum_{k=1}^{\infty}{}^{o}e_k R_0^k\frac{\zeta^{(k-1)}(z)}{(k-1)!}\right\},$$

$$\mathbf{X}^{(2)}(z)=\mathrm{Re}\left\{\sum_{k=1}^{\infty}{}^{o}c_k\frac{z^k}{R_0^k}\right\},\ \mathbf{Y}^{(2)}(z)=\mathrm{Re}\left\{\sum_{k=1}^{\infty}{}^{o}d_k\frac{z^k}{R_0^k}\right\},\ \mathbf{Z}^{(2)}(z)=\mathrm{Re}\left\{\sum_{k=1}^{\infty}{}^{o}f_k\frac{z^k}{R_0^k}\right\}.\quad \text{in } S_2 \quad (17)$$

In Eq. (16) and Eq. (17), it is necessary to highlight that the summation symbol with superscript "*o*" means that "*k*" runs only over odd integers, R_0 is the radio of the fiber in the composites, and the real or imaginary part of the complex number are represented by Re or Im respectively. The symbol $w_{kp}=(k+p-1)!\left[(k-1)!(p-1)!\right]^{-1}R_1^{k+p}\left(kp\right)^{-1/2}\sum_{m,n}(m\omega_1+n\omega_2)^{-(k+p)}$, with $m^2+n^2\neq 0,\ \ k+p\geq 2$ and by definition $S_2=0$. $\zeta(z)=z^{-1}+\sum_{m,n}{}'\left[\left(z-\beta_{mn}\right)^{-1}+\beta_{mn}^{-1}+z\beta_{mn}^{-2}\right]$

represent the Zeta quasi periodic Weierstrass function, which satisfies the quasi periodic conditions $\delta_\gamma = \zeta(z+\omega_\gamma) - \zeta(z)$ with $\beta_{mn} = m\omega_1 + n\omega_2$. The principal periods are ω_1 and ω_2, and $\sum_{m,n}'$ with the prime over the summation symbolizes that the summation runs for all $m, n \in Z$ excluding $(m, n) = (0, 0)$. The corresponding coefficients $a_0, a_k, b_0, b_k, e_0, e_k, c_k, d_k$ and f_k are undetermined complex numbers. They are different for each individual antiplane local problem. Only when we analyzed the square and hexagonal RVE, these coefficients are real. These particular cases can be seen in Espinosa Almeyda et al. (2011).

Finally, the solution of the local problems ${}_{13}\mathcal{L}$, ${}_{23}\mathcal{L}$, ${}_{1}\mathcal{I}$, ${}_{2}\mathcal{I}$, ${}_{1}\mathcal{P}$ and ${}_{2}\mathcal{P}$ is determinated by means of a system which is a result of substituting Eqs. (16) and (17) in to Eq. (14) (see Sixto-Camacho et al., 2013) and after some algebraic manipulations, we have

$$\begin{aligned}
&\mathcal{A}_{1p}\,\overline{a}_p - \mathcal{A}_{2p}\,E_p(a) + \mathcal{B}_{1p}\,\overline{b}_p - \mathcal{B}_{2p}\,E_p(b) + \mathcal{C}_{1p}\,\overline{e}_p - \mathcal{C}_{2p}\,E_p(e) = \mathrm{T}_1 R\delta_{1p}\left(\delta_{1\lambda} - i\delta_{2\lambda}\right),\\
&\mathcal{A}_{3p}\,\overline{a}_p - \mathcal{A}_{4p}\,E_p(a) + \mathcal{B}_{3p}\,\overline{b}_p - \mathcal{B}_{4p}\,E_p(b) + \mathcal{C}_{3p}\,\overline{e}_p - \mathcal{C}_{4p}\,E_p(e) = \mathrm{T}_2 R\delta_{1p}\left(\delta_{1\lambda} - i\delta_{2\lambda}\right),\\
&\mathcal{A}_{5p}\,\overline{a}_p - \mathcal{A}_{6p}\,E_p(a) + \mathcal{B}_{5p}\,\overline{b}_p - \mathcal{B}_{6p}\,E_p(b) + \mathcal{C}_{5p}\,\overline{e}_p - \mathcal{C}_{6p}\,E_p(e) = \mathrm{T}_3 R\delta_{1p}\left(\delta_{1\lambda} - i\delta_{2\lambda}\right),
\end{aligned} \tag{18}$$

where $E_p(f) = (f)_0\delta_{1p} - \sum_{k=1}^{\infty}{}^{o}(f)_k k^{1/2} p^{-1/2} w_{kp}$, and $R = R_0 / l$ is the dimensionless radius of the fiber. The independent terms are denoted by T_1, T_2 and T_3, and the coefficients $\mathcal{A}_{sp}$, $\mathcal{B}_{sp}$ and $\mathcal{C}_{sp}$ $(s = \overline{1,6})$ are dimensionless relations that are defined in Appendix A. The sum by the repeated indices k and p is applied, with $k, p = 1, 3, 5, \cdots$. The over bar indicates complex conjugate. The relation between the specific local problems and the independent terms is given in Table 2.

Table 2

It is important to notice that the right part of the system Eq. (18) is the same one for all antiplane local problems, only the left part is different. In addition, the involved series of w_{kp} are convergent and, consequently, the Eq. (18) is a normal infinite system of algebraic equations, which is solved by means of truncations (with N_0 as truncation order) to obtain approximations of the undetermined coefficients a_k, b_k and e_k. Larger orders of truncation give a better level of

ACCEPTED MANUSCRIPT

approximation. The complex solutions of Eq. (18) depend on the material constants, fiber distribution and volume fraction.

The simple analytical expression of the effective coefficients shown in Eq. (15) for the antiplane problems are deduced by applying the Green's theorem to the RVE area, taking into consideration Eq. (16) and Eq. (17), as well as the double periodicity of the local functions and the orthogonality of the system of functions $\{e^{in\theta}\}_{n=-\infty}^{\infty}$ with $0 \le \theta \le 2\pi$, where the dimensionless coefficients $E_{15}^{(1)}$, $Q_{15}^{(1)}$ and $A_{11}^{(1)}$ are summarized in Appendix A. A representation of them associated with ${}_{13}\mathcal{L}$ and ${}_{23}\mathcal{L}$ local problem is

$$
\begin{aligned}
&C_{1313}^{*} - iC_{2313}^{*} = 1 - \frac{\pi d}{\mathrm{V}}(\bar{a}_1 + E_{15}^{(1)}\,\bar{b}_1 + Q_{15}^{(1)}\,\bar{e}_1),\\
&\tilde{e}_{113}^{*} - i\tilde{e}_{213}^{*} = E_{15}^{(1)} - \frac{\pi d}{\mathrm{V}}(E_{15}^{(1)}\,\bar{a}_1 - \bar{b}_1 - A_{11}^{(1)}\,\bar{e}_1), \qquad \text{associated to the local problem } {}_{13}\mathsf{L} \qquad (19)\\
&\tilde{q}_{113}^{*} - i\tilde{q}_{213}^{*} = Q_{15}^{(1)} - \frac{\pi d}{\mathrm{V}}(Q_{25}^{(1)}\,\bar{a}_1 - A_{11}^{(1)}\,\bar{b}_1 - \bar{e}_1),
\end{aligned}
$$

$$
\begin{aligned}
&C_{3123}^{*} - iC_{3223}^{*} = -i - \frac{\pi d}{\mathrm{V}}(\bar{a}_1 + E_{25}^{(1)}\,\bar{b}_1 + Q_{15}^{(1)}\,\bar{e}_1),\\
&e_{123}^{*} - ie_{223}^{*} = -iE_{15}^{(1)} - \frac{\pi d}{\mathrm{V}}(E_{15}^{(1)}\,\bar{a}_1 - \bar{b}_1 - A_{11}^{(1)}\,\bar{e}_1), \qquad \text{associated to the local problem } {}_{23}\mathsf{L} \qquad (20)\\
&q_{123}^{*} - iq_{223}^{*} = -iQ_{15}^{(1)} - \frac{\pi d}{\mathrm{V}}(Q_{15}^{(1)}\,\bar{a}_1 - A_{11}^{(1)}\,\bar{b}_1 - \bar{e}_1),
\end{aligned}
$$

with d the diameter of the fibers and $\mathrm{V} = |\omega_1||\omega_2|\sin\theta_1$ the volume of the RVE. The remaining ones related to the rest of the local problems are showed in the Appendix B,

The analytical expressions of moduli effective coefficients are functions of the constituent material properties and the phase volume fraction, of periodic cell ω_1 and ω_2 by means of the systems solutions a_1, b_1 and e_1, corresponding to the associated local problem. The precision here is only based on the number of iterations. They are needed to achieve the convergence. Computation stops when the difference between the coefficients a_1, b_1 and e_1 for subsequent steps reaches the desired precision. These coefficients are substituted into the expressions Eqs. (19) and (20) in order to finally obtain the overall properties.

An important approximation from Eq. (18) is obtained if we consider $\mathrm{N}_0 = 1$. In this case, the only unknowns of the system are those whose subscripts k and p are equal to 1, and

ACCEPTED MANUSCRIPT

therefore, the solutions are easy to find. Here, the system (see Eq. (18)) is reduced in the matricial compact form as

$$\left(E+R^2J\right)X=R\Lambda, \tag{21}$$

where $X^T=\left(x_1 \quad y_1 \quad z_1 \quad t_1 \quad l_1 \quad m_1\right)$ is the transpose of the vector X, which contains the real and imaginary parts of the unknown $a_1=x_1+iy_1$, $b_1=z_1+it_1$ and $e_1=l_1+im_1$. The transpose of the independent vector Λ is given by $\Lambda^T=\left(\mathcal{A}_{21}\delta_{\lambda 1} \quad \mathcal{A}_{21}\delta_{\lambda 2} \quad \mathcal{A}_{41}\delta_{\lambda 1} \quad \mathcal{A}_{41}\delta_{\lambda 2} \quad \mathcal{A}_{61}\delta_{\lambda 1} \quad \mathcal{A}_{61}\delta_{\lambda 2}\right)$ for the ${}_{13}\mathcal{L}$ and ${}_{23}\mathcal{L}$ local problems, by $\Lambda^T=\left(\mathcal{B}_{21}\delta_{\lambda 1} \quad \mathcal{B}_{21}\delta_{\lambda 2} \quad \mathcal{B}_{41}\delta_{\lambda 1} \quad \mathcal{B}_{41}\delta_{\lambda 2} \quad \mathcal{B}_{61}\delta_{\lambda 1} \quad \mathcal{B}_{61}\delta_{\lambda 2}\right)$ for the ${}_1\mathcal{I}$ and ${}_2\mathcal{I}$ local problems, and by $\Lambda^T=\left(\mathcal{C}_{21}\delta_{\lambda 1} \quad \mathcal{C}_{21}\delta_{\lambda 2} \quad \mathcal{C}_{41}\delta_{\lambda 1} \quad \mathcal{C}_{41}\delta_{\lambda 2} \quad \mathcal{C}_{61}\delta_{\lambda 1} \quad \mathcal{C}_{61}\delta_{\lambda 2}\right)$ for the ${}_1\mathcal{I}$ and ${}_2\mathcal{I}$ local problems, with $\lambda=1$ for ${}_{13}\mathcal{L}$, ${}_1\mathcal{I}$, and ${}_1\mathcal{P}$, and $\lambda=2$, for ${}_{23}\mathcal{L}$, ${}_2\mathcal{I}$, and ${}_2\mathcal{P}$.

The matrices E and J have the following form

$$E=\begin{pmatrix} 1 & 0 & \mathcal{B}_{11} & 0 & \mathcal{C}_{11} & 0 \\ 0 & 1 & 0 & \mathcal{B}_{11} & 0 & \mathcal{C}_{11} \\ 1 & 0 & \mathcal{B}_{31} & 0 & \mathcal{C}_{31} & 0 \\ 0 & 1 & 0 & \mathcal{B}_{31} & 0 & \mathcal{C}_{31} \\ 1 & 0 & \mathcal{B}_{51} & 0 & \mathcal{C}_{51} & 0 \\ 0 & 1 & 0 & \mathcal{B}_{51} & 0 & \mathcal{C}_{51} \end{pmatrix},\quad J=\begin{pmatrix} \mathcal{A}_{21}\tilde{H}_1 & \mathcal{A}_{21}\tilde{H}_3 & \mathcal{B}_{21}\tilde{H}_1 & \mathcal{B}_{21}\tilde{H}_3 & \mathcal{C}_{21}\tilde{H}_1 & \mathcal{C}_{21}\tilde{H}_3 \\ -\mathcal{A}_{21}\tilde{H}_2 & \mathcal{A}_{21}\tilde{H}_4 & -\mathcal{B}_{21}\tilde{H}_2 & \mathcal{B}_{21}\tilde{H}_4 & -\mathcal{C}_{21}\tilde{H}_2 & \mathcal{C}_{21}\tilde{H}_4 \\ \mathcal{A}_{41}\tilde{H}_1 & \mathcal{A}_{41}\tilde{H}_3 & \mathcal{B}_{41}\tilde{H}_1 & \mathcal{B}_{41}\tilde{H}_3 & \mathcal{C}_{41}\tilde{H}_1 & \mathcal{C}_{41}\tilde{H}_3 \\ -\mathcal{A}_{41}\tilde{H}_2 & \mathcal{A}_{41}\tilde{H}_4 & -\mathcal{B}_{41}\tilde{H}_2 & \mathcal{B}_{41}\tilde{H}_4 & -\mathcal{C}_{41}\tilde{H}_2 & \mathcal{C}_{41}\tilde{H}_4 \\ \mathcal{A}_{61}\tilde{H}_1 & \mathcal{A}_{61}\tilde{H}_3 & \mathcal{B}_{61}\tilde{H}_1 & \mathcal{B}_{61}\tilde{H}_3 & \mathcal{C}_{61}\tilde{H}_1 & \mathcal{C}_{61}\tilde{H}_3 \\ -\mathcal{A}_{61}\tilde{H}_2 & \mathcal{A}_{61}\tilde{H}_4 & -\mathcal{B}_{61}\tilde{H}_2 & \mathcal{B}_{61}\tilde{H}_4 & -\mathcal{C}_{61}\tilde{H}_2 & \mathcal{C}_{61}\tilde{H}_4 \end{pmatrix},$$

where $\tilde{H}_1=\left(h_{11}+h_{12}\right)$, $\tilde{H}_2=\left(h_{21}+h_{22}\right)$, $\tilde{H}_3=\left(h_{21}-h_{22}\right)$ and $\tilde{H}_4=\left(h_{11}-h_{12}\right)$. Also,

$$h_{11}=\mathrm{Re}\left\{\frac{\bar{\delta}_1\bar{\omega}_2-\bar{\delta}_2\bar{\omega}_1}{\omega_1\bar{\omega}_2-\omega_2\bar{\omega}_1}\right\},\ h_{21}=\mathrm{Im}\left\{\frac{\bar{\delta}_1\bar{\omega}_2-\bar{\delta}_2\bar{\omega}_1}{\omega_1\bar{\omega}_2-\omega_2\bar{\omega}_1}\right\},\ h_{12}=\mathrm{Re}\left\{\frac{\delta_1\bar{\omega}_2-\delta_2\bar{\omega}_1}{\omega_1\bar{\omega}_2-\omega_2\bar{\omega}_1}\right\},\ h_{22}=\mathrm{Im}\left\{\frac{\delta_1\bar{\omega}_2-\delta_2\bar{\omega}_1}{\omega_1\bar{\omega}_2-\omega_2\bar{\omega}_1}\right\}$$

with $\delta_\gamma=2\zeta\ \omega_\gamma/2$ and $\bar{\delta}_\gamma$ is the conjugate of δ_γ. The coefficients $\mathcal{A}_{s1}$, $\mathcal{B}_{s1}$ and $\mathcal{C}_{s1}$ $(s=\overline{1,6})$ are defined in Appendix A, considering p equal to 1. In general, the system Eq. (21), for each local problem, is easily solved for the corresponding unknowns a_1, b_1 and e_1. Then, the effective coefficients showed in Eqs. (19) and (20), and in Appendix B are determinated.

ACCEPTED MANUSCRIPT

ACCEPTED MANUSCRIPT

4. Model validation and Numerical results

Limit cases for the present model can be obtained when the analytical expressions are reduced to those that describe a transversally isotropic two-phase composites with purely elastic or piezoelectric constituents and parallelogram-like RVE, such as the works reported by Guinovart-Díaz et al. (2011), (2012); López-Realpozo et al. (2011); Rodríguez-Ramos et al. (2011).

The numerical simulations were conducted for different cases of two-phase composites (fiber/matrix). The values of the elastic, piezoelectric, dielectric, piezomagnetic and magnetic properties used in the computations are shown in Table 3. The results are fundamentally verified through comparisons between the present model and the numerical results reported by: i) Wang and Pan (2007), which implement of Mori‐Tanaka self-consistent method; ii) Yang et al. (2013), development of the eigenfunction expansion-variational method; iii) Kuo (2011) mixed a method of complex potentials with a re-expansion formulae and the generalized Rayleigh's formulation on periodic conductive composites and iv) Xu and Xiao (2015) using the analytical method based on the average-field theory.

Table 3

The three-phase model (fiber/interphase/matrix) approach to describe the imperfect contact considering the interphase as a thin third phase between the matrix and the fiber has received attention in the literature Yan et al. (2013) and Espinosa-Almeyda et al. (2014). A first validation can be seen in Table 4. Here, comparisons of the present model with the above mentioned three-phase models and with analytical models for multicoated fibers developed by Kuo (2011) and Xu and Xiao (2015) are reported. The Yan et al. (2013) and Kuo (2011) three-phase models with doubly periodic microstructures assumed that the concentric fibers radius relation is 4/5. Herein, it is considered that the volume fraction for the fiber and the interphase are 0.6 and 10^{-6}, respectively.

As shown in table 4, the variations of the antiplane MEE effective properties are presented for a two-phase composite BTO/CFO (fiber/matrix) with different truncation orders of the system N_0, $(N_0 = 1, 3, 5, 7, 9)$ and with square RVE. Here, the BTO fiber volume fraction is 0.6 and the imperfect contact conditions at the interface are limited to the perfect case

ACCEPTED MANUSCRIPT

$(K = M = N = 0)$. Notice that the convergence of the present model is reached for smaller values of N_0, $(N_0 \leq 3)$. Truncations of higher order must be included for high volume fraction of fibers as well as for higher contrast between the fiber and matrix. Good match among the approaches can be observed.

Table 4

Fig. 2(a) and (b) illustrate the effective ME coefficients $\alpha_{11}^* = \alpha_{22}^*$ versus the fiber volume fraction V_2 for the two-phase composites: CFO/BTO and TD/BTO, respectively. In both figures, perfect contact conditions at interface, and square or hexagonal RVEs are considered. The obtained values by AHM are compared up to the maximum allowed fiber volume fraction (percolation) with those given by Wang and Pan, (2007) when the RVE is only hexagonal and by Yan et al., (2013), when the RVEs are hexagonal and square. The accuracy with the values reported by Wang and Pan (2007) are obtained for a first truncate order $(N_0 = 1)$ of the system Eq. (18). The truncation order $N_0 = 9$ allows the AHM numerical precision to reproduce the results given by Yan et al., (2013).

In both Figs. 2(a) and 2(b), the respective maximum allowable fiber volume fractions are 0.7853 for square RVE and 0.906 for a hexagonal RVE. Note that, for small values of V_2, the type of RVEs (square or hexagonal) does not impact on α_{11}^*, it is the same value in both RVEs. However, when V_2 increases, the effect of the RVE is significant and it is more noteworthy in a TD/BTO composite (Fig. 2(b)). Near the percolation, the property has notable changes. For a composite CFO/BTO (see Fig. 2(a)), it is seen that, the ME property weakens after reaching the highest magnitude when $V_2 \approx 0.76$ for a square RVE; $V_2 \approx 0.84$ for a hexagonal RVE and $V_2 \approx 0.86$ for the estimation compared with Wang and Pan (2007). For a TD/BTO composite (see Fig. 2(b)), the ME property increases considerably up to the fiber percolation. This drastic change in the magnetoelectric property is also reported by Yan et al., (2013). They argue that when fibers contact together at percolation, the matrix is separated by the fibers, then the matrix that was a continuous phase before fiber percolation becomes a discontinuous phase and the

ACCEPTED MANUSCRIPT

initially disperse fibers form a continuous phase. Therefore a sudden change of the magnetoelectric coefficient is something possible. Higher values are reached for the square RVE. After that, some local extreme values are reaches for $V_2 \approx 0.4193$ and $V_2 \approx 0.5790$ when the RVE is square and $V_2 \approx 0.3794$ and $V_2 \approx 0.8586$ when the RVE is hexagonal.

In Fig. 3, the effective ME property α_{11}^{*} for different two-phase composites versus the fiber volume fraction are depicted for a hexagonal RVE, under perfect contact conditions at interface. Here, four two-phase composites made of combinations of CFO, BTO and TD are analyzed. Comparison between the values obtained by the present model with those reported by Yan et al., (2013) is presented. The estimations illustrated in Fig. 3 show that the numerical values obtained by the models are coincident. From Fig. 3, it is seen that the ME property α_{11}^{*} of the BTO/TD composite is much large than those of the other constituent combinations and different behaviour for α_{11}^{*} are observed when the components are exchanged. Additionally, in composites with BTO as matrix and CFO or TD as fiber, a higher ME coupling property α_{11}^{*} is obtained when the fiber is made of TD. We should notice that the ME coupling property depends on the piezoelectric and piezomagnetic properties, as well as the jump of the mechanic property. In this sense, the piezomagnetic property of the CFO is bigger than that of the TD; then, the evident increase of α_{11}^{*} is due to the jump of the mechanical property at interface.

The analysis developed in Table 4, Figs. 2 and 3 allows us to illustrate, as a particular case, the phenomena of the interface imperfection by means of the effect of a thin interphase. The approaches obtained by the different models show the accuracy and the efficiency of the employed method.

In Table 5, we present the overall MEE properties for two-phase composite (BTO/CFO) under perfect contact for different parallelogram-like fiber distribution, (i.e., different RVEs with respective inclination angle θ_1 equal to 45°, 50°, 60°, 70°, 75°, 80° and 90° - see Fig. 1(b)). The values are computed considering $V_2 = 0.6$ and $N_0 = 9$. The present model allows analyzing the structure-property relationship. Consequently, the composite belongs to monoclinic symmetric class characterized by 18 different homogenized coefficients derived from the RVE, when it is

ACCEPTED MANUSCRIPT

different from the hexagonal (60°) and square (90°) RVEs. Only for hexagonal and square RVEs, the global properties of the composites are transversely isotropic, i.e., the property relations $C^*_{1313} = C^*_{2323}$, $e^*_{113} = e^*_{223}$, $q^*_{113} = q^*_{223}$, $\kappa^*_{11} = \kappa^*_{22}$, $\alpha^*_{11} = \alpha^*_{22}$ and $\mu^*_{11} = \mu^*_{22}$, are satisfied and the rest of the coefficients are null. From Table 5, it is important to note that, for the same fiber volume fraction and for the RVE angle, θ_1, less than 60°, the properties have notable differences, not being like that when the RVE angle are higher than 60°. These differences in the properties must be a result of the axial symmetry changes due to the spatial fiber distribution. The interactions between neighboring fibers, because of the specific geometry of the structure, have a strong influence in the overall behaviour of the material. Also, it is observed that the properties C^*_{1323}, e^*_{123}, q^*_{123}, κ^*_{12}, α^*_{12} and μ^*_{12} are more sensitive to the geometry of the RVE that the remaining ones, when the angle changes.

The imperfect contact condition effects on the effective properties are also discussed below. In Fig. 4, the ME effective property α^*_{11} of a BTO/CFO (fiber/matrix) composite versus the fiber volume of fraction V_2 is given. Here, the influence of various parallelogram-like RVE (as seen, RVEs with the θ_1 angle equal to 45°, 60°, 75°, 80° and 90°) on the property α^*_{11} is analyzed. Only two different mechanical imperfections K characterized by $K = 0.45$ and $K = 10$ with $M = N = 0$ are considered. The numerical values are determinated for a first order of truncation $(N_0 = 1)$ of the system (Eq. (18)). For the hexagonal RVE, a comparison between the Present model (AHM - 60°) and Wang and Pan (2007) models are shown until the fiber percolation.

From Fig. 4, we can conclude that the ME coefficient decreases as consequence of the growing effect of the mechanical imperfection. This result is congruent with those reported by Wang and Pan (2007). Hence, the contact imperfection and the fiber distribution have a pronounced effect on α^*_{11}. Here, the weakest values are obtained when the fibers has a hexagonal distribution. In this case, the property α^*_{11} continually grows until their maximum values and then falls down.

For the rest of RVE types, the different lines of α_{11}^{*} have very light changes of concavity, and finally, they increase quickly until V_2 reaches the percolation limit. For $\theta_1 = 45°$, the ME coefficient, α_{11}^{*}, has the highest values in comparison to the rest of the θ_1 values in the same volume fraction interval. When the angle θ_1 is in the range $60° < \theta_1 \leq 90°$, the behaviors of the curves of all coefficients are similar, the differences are remarkable near the maximum percolation point. In that point, as seen, the differences are reduce when the imperfection is bigger.

In Fig.5, different fiber volume fraction curves of the normalized ME effective coefficient α_{11}^{*} computed by AHM model for a periodic hexagonal cell versus different mechanical imperfections K (Fig. 5(a)), electrical imperfection M (Fig. 5(b)) and magnetical imperfection N (Fig. 5(c)) are displayed. The numerical calculations are carried out for a two-phase (BTO/CFO) composite for different fiber volume fractions to the percolation volume $V_2 = 0.906$, and for a first truncate orders $N_0 = 1$ of system Eq. (18). Here, the ME property decreases as consequence of the mechanical, electrical and magnetical imperfections growth. Besides, for each imperfection type, the normalized ME dependence for the percolation acts as a lower limit. The normalization of α_{11}^{*} is relative to the perfect contact case.

For Fig.5(a), it is worthily to notice that a reasonable coincidence has been achieved for almost all the curves with the exception of those where the fiber volume fraction is less than 0.15. According to the definition of K starting from $\hat{K}$, K must be an intensive parameter in the formal thermodynamic sense. The coincidences of the curves in Figs. 5(a) and 5(c) mean that the effect of the fiber volume fraction is almost negligible on the dependence on the normalized magnetoelectric coefficient. Hence, this is the adequate dependence to quantify the effect of K on α_{11}^{*}. The maximum values of α_{11}^{*} are obtained when $K = 0$, which corresponds to the perfect contact.

As an example, it can be seen that for $K = 1.5$, the ME coefficient loses the 50% of its value, and for $K = 5$, it loses the 80%. This is a valid result for all the fiber volume fraction values under a good approximation (see Fig. 5(a)). For $N = 1$, the ME coefficient loses the 50% and for $N = 4.2$, it loses the 80% no matter what the value of the fiber volume fraction is (see

ACCEPTED MANUSCRIPT

ACCEPTED MANUSCRIPT

Fig. 5(c)). However, it is not possible to systematize the effect of the M parameter on the ME coupling as can be seen in Fig. 5 (b) since the weakening of the ME depends on the fiber volume fraction. Further research focused on the systematization of the imperfect contact parameter is needed.

Fig. 6 illustrates the dependence of the ME coupling coefficient α_{11}^{*} as function of the electrical and magnetical imperfections M and N, respectively. It can be observed for the composite CFO/BTO (Fig. 6 (a)) that the ME coefficient weakening is more sensitive to the electrical imperfection M than the magnetical imperfection. For the composite TD/BTO (Fig. 6(b)), the ME coefficient intensely decrease as both the electrical and magnetical imperfections get stronger.

In Table 6, the mechanical, electrical and magnetical imperfection influence on the ME coefficients α_{11}^{*}, α_{12}^{*} and α_{22}^{*} are illustrated. The values are reported for a CFO/BTO composite when hexagonal, square and parallelogram-like with $\theta_1 = 75°$ the RVEs are considered. Here, the CFO volume fraction is 0.6 and the truncate order of the system Eq. (18) is $N_0 = 1$. In addition, a comparison between Wang and Pan (2007) and AHM models for hexagonal RVE is displayed. From Table 6, we concluded that, for each combination of the imperfect parameters K, M and N, it is possible to see that the properties α_{11}^{*}, α_{12}^{*} and α_{22}^{*} decrease as any kind of imperfection appears. Note that, when the RVE is hexagonal or square, the coefficient α_{11}^{*} is the only one reported. It is due to the transversely isotropic symmetry of the composite (the coefficients $\alpha_{11}^{*} = \alpha_{22}^{*}$ and $\alpha_{12}^{*} = 0$), as reported by Yan et al. (2013). For the parallelogram-like RVE with $\theta_1 = 75°$, the effective coefficients α_{12}^{*} and α_{21}^{*} are non-null and coincident. The last result is due to the fact that the composite exhibits a monoclinic symmetry. In addition, it is necessary to notice that under the effects of the imperfect contact conditions for the three types parallelogram-likes RVE, the ME maximum values are reached when the RVE is square.

In Table 7, the complete magneto-electro-elastic moduli for two parallelogram-like RVEs under different type of imperfection are presented. The Table 7 RVE angles are $\theta_1 = 45°$ and $\theta_1 = 75°$. The imperfections sets are varied in five combinations: perfect contact

ACCEPTED MANUSCRIPT

($K = M = N = 0$), only mechanical imperfection ($K = 10$ and $M = N = 0$), only electrical imperfection ($M = 10$ and $K = N = 0$), only magnetical imperfection ($N = 10$ and $K = M = 0$), and a total imperfection ($K = M = N = 10$). From Table 7, it can be seen how the properties are sensitive under the different imperfection effects. Notice that some properties are more sensitive to an imperfection type than the other ones, and even for the properties C^*_{2313}, e^*_{213}, q^*_{213}, κ^*_{12}, α^*_{12}, and μ^*_{12}, the signs change. This is because of the transversely orthotropic behavior associated with the inclination, θ_1, of the RVE. The Table 8 complements the results reported in Table 7.

In Table 8, a general summary of the different imperfection effects on the magneto-electro-elastic properties for two composites (BTO/CFO and CFO/BTO) with parallelogram-like RVE is given. As we can see, the properties are grouped according to whether they are affected or not by an specific type of imperfection.

From Tables 7 and 8, it is possible to conclude that: i) the parallelogram-like RVE, i.e., fiber array have always influence on the MEE effective properties regardless of the presence or kind of imperfection; ii) The imperfection effect on the properties, summarized in Table 8, does not depend on the kind of the RVE; iii) The magnetoelectric coupling properties (α^*_{11}, α^*_{12} and α^*_{22}) are always affected by any of the situations studied herein, as type of imperfection, fiber distribution or change of constituent; iv) The effective piezomagnetic (piezoelectric) coupling is not affected by any kind of imperfect contact when the matrix is made of the piezomagnetic (piezoelectric) constituent; v) The effective piezoelectric (piezomagnetic) coupling is affected when the fiber is made of the piezoelectric (piezomagnetic) constituent and the electrical (magnetic) imperfection is present. For these cases, the mechanical imperfection always affects the coupling; vi) The effective elastic property C^*_{2323} is affected when the matrix is made of piezoelectric constituent and the electrical imperfection is present; the underlined coefficients (C^*_{1313} and C^*_{2323}) are affected only near the percolation point under the same previous conditions.

In Fig. 7, the MEE effective properties for a porous composite are given. Herein, the numerical fulfillment of the exact relations $\frac{C^*_{1313}}{C^{(1)}_{1313}}=\frac{e^*_{113}}{e^{(1)}_{113}}=\frac{q^*_{113}}{q^{(1)}_{113}}=\frac{\kappa^*_{11}}{\kappa^{(1)}_{11}}=\frac{\mu^*_{11}}{\mu^{(1)}_{11}}$, $\frac{C^*_{2323}}{C^{(1)}_{1313}}=\frac{e^*_{223}}{e^{(1)}_{113}}=\frac{q^*_{223}}{q^{(1)}_{113}}=\frac{\kappa^*_{22}}{\kappa^{(1)}_{11}}=\frac{\mu^*_{22}}{\mu^{(1)}_{11}}$ and $\frac{C^*_{2313}}{C^{(1)}_{1313}}=\frac{e^*_{213}}{e^{(1)}_{113}}=\frac{q^*_{213}}{q^{(1)}_{113}}=\frac{\kappa^*_{12}}{\kappa^{(1)}_{11}}=\frac{\mu^*_{12}}{\mu^{(1)}_{11}}$, obtained by Sixto-Camacho et al., (2015) for porous fiber composite, was demonstrated. In addition, the relations (3.6)-(3.15) from Sixto-Camacho et al., (2015) are also satisfied. Hence, each curve of Fig. 7 describes all the normalized properties shown in the $Oy-$axes for a specific θ_1. The porosity is represented by empty fibers periodically distributed in a homogeneous and transversely isotropic matrix. The porosity distribution is defined by a parallelogram-like array as REV. These relations are applicable for any kind of RVE with empty-fiber. Note that, the curves for each porosity distribution are monotonically decreasing from the normalized matrix value to the allowed lower value that corresponds to the percolation limit. This effect of the weakening of the properties is due to the fact that the pore size increases. As validation, in Fig. 7(a), a comparison with the results reported by Bravo-Castillero et al. (2009) when $\theta_1=90^\circ$ is showed. The curves illustrate a total coincidence for $BaTiO_3$ porous material.

5. Conclusions

In this work, an approach using the asymptotic homogenization method for estimating the antiplane effective properties of two-phase piezoelectric–piezomagnetic fiber reinforced composites with imperfect fiber-matrix interface and parallelogram-like fiber arrangement is proposed. The analytical formulae derived for the antiplane general local problems, their solutions and the corresponding effective coefficients have a simple form and are of easy computational implementation. Also, the formulae are also valid for studying the interface problem of two-phase piezoelectric or elastic composite. The accuracy and efficiency of the present method were tested with the existing analytical results and for all the comparisons, good approximations were obtained. Regarding the numerical result, we have come to the conclusion that:

ACCEPTED MANUSCRIPT

i) The manipulation of the fiber distribution, represented as parallelogram-like RVEs, allows two class of symmetry point group for the composite global behavior: monoclinic 2 and transversely isotropic structure.

ii) The moduli of effective properties are either influenced or not depending on the type of the contact imperfection, i.e., here interpreted as linear spring K, an electrical capacitance M and a magnetic inductance N, and the set of materials constituents.

iii) The magnetoelectric coupling is sensitive to the fiber distribution, the type of imperfection and the combination of constituents.

iv) The effect of the imperfection is dominant over the spatial fiber distribution. The imperfect contact conditions considerable changes the values of the ME coefficients. While, the fiber distribution induces weaker changes in the ME coupling and, sometimes, the appearance of new components (monoclinic 2). Each of these effects can be studied separately.

v) The connection between the imperfect contact parameters and the weakening of ME coefficient cannot always be established as an independent function on the composite structure. More systematization is needed in this sense.

vi) This approximation is capable of describing the porosity behaviour in a proper way.

Acknowledgements

Y. Espinosa-Almeyda would like to thank CONACYT for a scholarship funding. The authors are grateful for the sabbatical stay of J. C. López-Realpozo supported by CONACYT grant number 253087 at Universidad Autónoma de Ciudad Juárez under the call "Estancias Sabáticas en México para Mexicanos y Extranjeros Residentes en el Exterior para la Consolidación de Grupos de Investigación"

Appendix A

The magnitudes involved in the systems Eq. (18) are summarized

$$\mathsf{A}_{1p}=1,\ \mathsf{A}_{2p}=\left(1-\chi^{*}+pK\chi^{*}-E_{15}^{(1)}E_{15}^{(2)}\sqrt{\chi^{*}\kappa^{*}}\,pM-Q_{15}^{(1)}Q_{15}^{(2)}\sqrt{\chi^{*}\mu^{*}}\,pN\right)/\beta_{p},\ \mathsf{A}_{3p}=1,$$

$$\mathsf{A}_{4p}=\left(E_{15}^{(1)}-E_{15}^{(2)}\sqrt{\chi^{*}\kappa^{*}}+E_{15}^{(2)}\sqrt{\chi^{*}\kappa^{*}}\,pK+\kappa^{*}E_{15}^{(1)}\,pM+Q_{15}^{(1)}A_{11}^{(2)}\sqrt{\kappa^{*}\mu^{*}}\,pN\right)/\alpha_{p},\ \mathsf{A}_{5p}=1,$$

ACCEPTED MANUSCRIPT

$$\mathcal{A}_{6p}=\left(Q_{15}^{(1)}-Q_{15}^{(2)}\sqrt{\chi^*\mu^*}+Q_{15}^{(2)}\sqrt{\chi^*\mu^*}\,pK+E_{15}^{(1)}A_{11}^{(2)}\sqrt{\kappa^*\mu^*}\,pM+Q_{15}^{(1)}\mu^*\,pN\right)/\gamma_p,$$

$$\mathcal{B}_{1p}=\left(E_{15}^{(1)}+E_{15}^{(2)}\sqrt{\chi^*\kappa^*}+E_{15}^{(1)}\chi^*\,pK+E_{15}^{(2)}\sqrt{\chi^*\kappa^*}\,pM+A_{11}^{(1)}Q_{15}^{(2)}\sqrt{\chi^*\mu^*}\,pN\right)/\beta_p,$$

$$\mathcal{B}_{2p}=\left(E_{15}^{(1)}-E_{15}^{(2)}\sqrt{\chi^*\kappa^*}+E_{15}^{(1)}\chi^*\,pK+E_{15}^{(2)}\sqrt{\chi^*\kappa^*}\,pM+A_{11}^{(1)}Q_{15}^{(2)}\sqrt{\chi^*\mu^*}\,pN\right)/\beta_p,$$

$$\mathcal{B}_{3p}=\left(-1-\kappa^*+E_{15}^{(1)}E_{15}^{(2)}\sqrt{\chi^*\kappa^*}\,pK-\kappa^*\,pM-A_{11}^{(1)}A_{11}^{(2)}\sqrt{\kappa^*\mu^*}\,pN\right)/\alpha_p,$$

$$\mathcal{B}_{4p}=\left(-1+\kappa^*+E_{15}^{(1)}E_{15}^{(2)}\sqrt{\chi^*\kappa^*}\,pK-\kappa^*\,pM-A_{11}^{(1)}A_{11}^{(2)}\sqrt{\kappa^*\mu^*}\,pN\right)/\alpha_p,$$

$$\mathcal{B}_{5p}=\left(-A_{11}^{(1)}-A_{11}^{(2)}\sqrt{\kappa^*\mu^*}+E_{15}^{(1)}Q_{15}^{(2)}\sqrt{\chi^*\mu^*}\,pK-A_{11}^{(2)}\sqrt{\kappa^*\mu^*}\,pM-A_{11}^{(1)}\mu^*\,pN\right)/\gamma_p,$$

$$\mathcal{B}_{6p}=\left(-A_{11}^{(1)}+A_{11}^{(2)}\sqrt{\kappa^*\mu^*}+E_{15}^{(1)}Q_{15}^{(2)}\sqrt{\chi^*\mu^*}\,pK-A_{11}^{(2)}\sqrt{\kappa^*\mu^*}\,pM-A_{11}^{(1)}\mu^*\,pN\right)/\gamma_p,$$

$$\mathcal{C}_{1p}=\left(Q_{15}^{(1)}+Q_{15}^{(2)}\sqrt{\chi^*\mu^*}+Q_{15}^{(1)}\chi^*\,pK+A_{11}^{(1)}E_{15}^{(2)}\sqrt{\chi^*\kappa^*}\,pM+Q_{15}^{(2)}\sqrt{\chi^*\mu^*}\,pN\right)/\beta_p,$$

$$\mathcal{C}_{2p}=\left(Q_{15}^{(1)}-Q_{15}^{(2)}\sqrt{\chi^*\mu^*}+Q_{15}^{(1)}\chi^*\,pK+A_{11}^{(1)}E_{15}^{(2)}\sqrt{\chi^*\kappa^*}\,pM+Q_{15}^{(2)}\sqrt{\chi^*\mu^*}\,pN\right)/\beta_p,$$

$$\mathcal{C}_{3p}=\left(-A_{11}^{(1)}-A_{11}^{(2)}\sqrt{\kappa^*\mu^*}+Q_{15}^{(1)}E_{15}^{(2)}\sqrt{\chi^*\kappa^*}\,pK-A_{11}^{(1)}\kappa^*\,pM-A_{11}^{(2)}\sqrt{\kappa^*\mu^*}\,pN\right)/\alpha_p,$$

$$\mathcal{C}_{4p}=\left(-A_{11}^{(1)}+A_{11}^{(2)}\sqrt{\kappa^*\mu^*}+Q_{15}^{(1)}E_{15}^{(2)}\sqrt{\chi^*\kappa^*}\,pK-A_{11}^{(1)}\kappa^*\,pM-A_{11}^{(2)}\sqrt{\kappa^*\mu^*}\,pN\right)/\alpha_p,$$

$$\mathcal{C}_{5p}=\left(-1-\mu^*+Q_{15}^{(1)}Q_{15}^{(2)}\sqrt{\chi^*\mu^*}\,pK-A_{11}^{(1)}A_{11}^{(2)}\sqrt{\kappa^*\mu^*}\,pM-\mu^*\,pN\right)/\gamma_p,$$

$$\mathcal{C}_{6p}=\left(-1+\mu^*+Q_{15}^{(1)}Q_{15}^{(2)}\sqrt{\chi^*\mu^*}\,pK-A_{11}^{(1)}A_{11}^{(2)}\sqrt{\kappa^*\mu^*}\,pM-\mu^*\,pN\right)/\gamma_p,$$

being $\beta_p=1+\chi^*+pK\chi^*-p\sqrt{\chi^*\kappa^*}\,E_{15}^{(1)}E_{15}^{(2)}M-p\sqrt{\chi^*\mu^*}\,Q_{15}^{(1)}Q_{15}^{(2)}N$, $E_{15}^{(\alpha)}=e_{113}^{(\alpha)}/\sqrt{C_{1313}^{(\alpha)}\kappa_{11}^{(\alpha)}}$,

$\alpha_p=E_{15}^{(1)}+\sqrt{\chi^*\kappa^*}\,E_{15}^{(2)}\left(1+pK\right)+p\kappa^*E_{15}^{(1)}M+p\sqrt{\kappa^*\mu^*}\,Q_{15}^{(1)}A_{11}^{(2)}N$, $Q_{15}^{(\alpha)}=q_{113}^{(\alpha)}/\sqrt{C_{1313}^{(\alpha)}\mu_{11}^{(\alpha)}}$,

$\gamma_p=Q_{15}^{(1)}+\sqrt{\chi^*\mu^*}\,Q_{15}^{(2)}\left(1+pK\right)+p\sqrt{\kappa^*\mu^*}\,E_{15}^{(1)}A_{11}^{(2)}M+p\mu^*Q_{15}^{(1)}N$, $A_{11}^{(\alpha)}=\alpha_{11}^{(\alpha)}/\sqrt{\kappa_{11}^{(\alpha)}\mu_{11}^{(\alpha)}}$,

$\alpha^*=\alpha_{\alpha\alpha}^{(2)}/\alpha_{\alpha\alpha}^{(1)}$, $\kappa^*=\kappa_{\alpha\alpha}^{(2)}/\kappa_{\alpha\alpha}^{(1)}$, $\chi^*=C_{\alpha3\alpha3}^{(2)}/C_{\alpha3\alpha3}^{(1)}$ and $\mu^*=\mu_{\alpha\alpha}^{(2)}/\mu_{\alpha\alpha}^{(1)}$, $(\alpha=1,2)$.

The majority of the previous magnitudes of the dimensionless problems was obtained by means of the transformations reported by Wang and Ding (2006).

Appendix B

ACCEPTED MANUSCRIPT

ACCEPTED MANUSCRIPT

The simple analytical expression of the remaining effective coefficients corresponding to the antiplane local problems ${}_1\mathcal{I}$, ${}_1\mathcal{P}$, ${}_2\mathcal{I}$ and ${}_2\mathcal{P}$ are given

$$\tilde{e}^*_{113} - i\tilde{e}^*_{123} = E^{(1)}_{15} - \frac{\pi d}{\mathrm{V}}({}_1\bar{a}_1 + E^{(1)}_{15}\,{}_1\bar{b}_1 + Q^{(1)}_{15}\,{}_1\bar{e}_1),$$

$$\tilde{\kappa}^*_{11} - i\tilde{\kappa}^*_{21} = 1 + \frac{\pi d}{\mathrm{V}}(E^{(1)}_{15}\,{}_1\bar{a}_1 - {}_1\bar{b}_1 - A^{(1)}_{11}\,{}_1\bar{e}_1), \qquad \text{associated to the local problem } {}_1\mathcal{I},$$

$$\tilde{\alpha}^*_{11} - i\alpha^*_{21} = A^{(1)}_{11} + \frac{\pi d}{\mathrm{V}}(Q^{(1)}_{15}\,{}_1\bar{a}_1 - A^{(1)}_{11}\,{}_1\bar{b}_1 - {}_1\bar{e}_1),$$

$$\tilde{e}^*_{213} - i\tilde{e}^*_{223} = -iE^{(1)}_{25} - \frac{\pi d}{\mathrm{V}}({}_2\bar{a}_1 + E^{(1)}_{15}\,{}_2\bar{b}_1 + Q^{(1)}_{15}\,{}_2\bar{e}_1),$$

$$\tilde{\kappa}^*_{12} - i\tilde{\kappa}^*_{22} = -i + \frac{\pi d}{\mathrm{V}}(E^{(1)}_{15}\,{}_2\bar{a}_1 - {}_2\bar{b}_1 - A^{(1)}_{22}\,{}_2\bar{e}_1), \qquad \text{associated to the local problem } {}_2\mathcal{I},$$

$$\alpha^*_{12} - i\alpha^*_{22} = -iA^{(1)}_{22} + \frac{\pi d}{\mathrm{V}}(Q^{(1)}_{25}\,{}_2\bar{a}_1 - A^{(1)}_{22}\,{}_2\bar{b}_1 - {}_2\bar{e}_1),$$

$$\tilde{q}^*_{113} - i\tilde{q}^*_{123} = Q^{(1)}_{15} - \frac{\pi d}{\mathrm{V}}({}_1\bar{a}_1 + E^{(1)}_{15}\,{}_1\bar{b}_1 + Q^{(1)}_{25}\,{}_1\bar{e}_1),$$

$$\alpha^*_{11} - i\alpha^*_{21} = A^{(1)}_{11} + \frac{\pi d}{\mathrm{V}}(E^{(1)}_{15}\,{}_1\bar{a}_1 - {}_1\bar{b}_1 - A^{(1)}_{11}\,{}_1\bar{e}_1), \qquad \text{associated to the local problem } {}_1\mathcal{P},$$

$$\tilde{\mu}^*_{11} - i\tilde{\mu}^*_{21} = 1 + \frac{\pi d}{\mathrm{V}}(Q^{(1)}_{15}\,{}_1\bar{a}_1 - A^{(1)}_{22}\,{}_1\bar{b}_1 - {}_1\bar{e}_1),$$

$$\tilde{q}^*_{213} - i\tilde{q}^*_{223} = -iQ^{(1)}_{25} - \frac{\pi d}{\mathrm{V}}({}_2\bar{a}_1 + E^{(1)}_{25}\,{}_2\bar{b}_1 + Q^{(1)}_{25}\,{}_2\bar{e}_1),$$

$$\tilde{\alpha}^*_{12} - i\tilde{\alpha}^*_{22} = -iA^{(1)}_{22} + \frac{\pi d}{\mathrm{V}}(E^{(1)}_{15}\,{}_2\bar{a}_1 - {}_2\bar{b}_1 - A^{(1)}_{11}\,{}_2\bar{e}_1), \qquad \text{associated to the local problem } {}_2\mathcal{P}.$$

$$\tilde{\mu}^*_{12} - i\tilde{\mu}^*_{22} = -i + \frac{\pi d}{\mathrm{V}}(Q^{(1)}_{25}\,{}_2\bar{a}_1 - A^{(1)}_{22}\,{}_2\bar{b}_1 - {}_2\bar{e}_1),$$

References

Aboudi, J., 2001. Micromechanical analysis of fully coupled electro-magneto-thermo-elastic multiphase composites. Smart Mater. Struct. 10, 867–877.

Bakhvalov N.S., Panasenko G.P., 1989. Homogenization averaging processes in periodic media. Dordrecht: Kluwer.

ACCEPTED MANUSCRIPT

ACCEPTED MANUSCRIPT

Benveniste, Y., 1987. A new approach to the application of Mori–Tanaka's theory in composite materials. Mech. Mater. 6, 147–157.

Benveniste, Y., 1995. Magnetoelectric effect in fibrous composites with piezoelectric and piezomagnetic phases. Phys. Rev. B 51(22), 16424–16427.

Benveniste, Y., Miloh, T., 2001. Imperfect soft and stiff interfaces in two-dimensional elasticity. Mech. Mater. 33, 309–323.

Bravo-Castillero, J., Rodríguez-Ramos, R., Guinovart-Díaz, R., Sabina, F.J., Aguiar, A.R., Silva, U.P., Gómez-Muñoz, J.L., 2009. Analytical formulae for electromechanical effective properties of 3-1 longitudinally porous piezoelectric materials. Acta Mater. 57, 795‑803.

Bunget, I., Raetchi, V., 1981. Magnetoelectric Effect in the Heterogeneous System NiZn Ferrite-PZT Ceramic. Phys. Stat. Sol. 63(a), K55–K57.

Dinzart, F., Sabar, H., 2011. Magneto-electro-elastic coated inclusion problem and its application to magnetic-piezoelectric composite materials. Int. J. Solids Struct. 48, 2393–2401.

Eshelby, J.D., 1957. The determination of the elastic field of an ellipsoidal inclusion, and related problems. Proc. R. Soc. London, Ser. A 241, 376–396.

Espinosa-Almeyda, Y., López-Realpozo, J.C., Rodríguez-Ramos, R., Bravo-Castillero, J., Guinovart-Díaz, R., Camacho-Montes, H., Sabina, F.J., 2011. Effects of interface contacts on the magneto-electro-elastic coupling for fiber reinforced. Int. J. Solids Struct. 48, 1525–1533.

Espinosa-Almeyda, Y., Rodríguez-Ramos, R., Guinovart-Díaz, R., Bravo-Castillero, J., López-Realpozo, J.C., Camacho-Montes, H., Sabina, F.J., Lebon, F., 2014. Antiplane magneto-electro-elastic effective properties of three-phase fiber composite. Int. J. Solids Struct. 51, 3508–3521.

ACCEPTED MANUSCRIPT

ACCEPTED MANUSCRIPT

Guinovart-Díaz, R., López-Realpozo, J.C., Rodríguez-Ramos, R., Bravo-Castillero, J., Ramírez, M., Camacho-Montes, H., Sabina, F.J., 2011. Influence of parallelogram cells in the axial behaviour of fibrous composite. Int. J. Eng. Sci. 49, 75–84.

Guinovart-Díaz, R., Yan, P., Rodríguez-Ramos, R., López-Realpozo, J.C., Jiang, C.P., Bravo-Castillero, J., Sabina, F.J., 2012. Effective properties of piezoelectric composites with parallelogram periodic cell. Int. J. Eng. Sci. 53, 58-66.

Guinovart-Díaz, R., Rodríguez-Ramos, R., Bravo-Castillero, J., López-Realpozo, J.C., Sabina, F.J., Sevostianov, I., 2013a. Plane Magneto-Electro-Elastic Moduli of Fiber Composites with Interphase. Mech. Adv. Mater. Struct. 20, 552–563.

Harshe, G., Dougherty, J.P., Newnham, R.E., 1993. Theoretical modelling of 3-0, 0-3 magneto-electric composites. Int. J. Appl. Electromagnet. Mech. 4(2), 161-171.

Hashin, Z., 1990. Thermoelastic properties of fiber composites with imperfect interface. Mech. Mater. 8(4), 333–348.

Hashin, Z., 1991. The spherical inclusion with imperfect interface. J. Appl. Mech. 58(2), 444–449.

Hashin, Z., 2002. Thin interphase/imperfect interface in elasticity with application to coated fiber composites. J. Mech. Phys. Solids 50(12), 2509 – 2537.

Kuo, H.Y., 2011. Multicoated elliptic fibrous composites of piezoelectric and piezomagnetic phases. Int. J. Eng. Sci. 49, 561–575.

Kuo, H.Y., 2014. Fibrous composites of piezoelectric and piezomagnetic phases: Generalized plane strain with transverse electromagnetic fields. Mech. Mater. 75, 103–110.

ACCEPTED MANUSCRIPT

Kuo, H.Y., Chen, C.Y., 2015. Decoupling transformation for piezoelectric–piezomagnetic fibrous composites with imperfect interfaces. Int. J. Solids Struct. 54, 111-120.

Kuo, H.Y., Huang, T.Y., 2016. Effective moduli of multiferroic fibrous composites with spring-type imperfect interfaces under generalized plane strain with transverse electromagnetic fields. Int. J. Solids Struct. 80, 456-464.

Li, J.Y. and Dunn, M.L., 1998. Micromechanics of Magnetoelectroelastic Composite Materials: Average Fields and Effective Behavior. J. Intell. Mater. Syst. Struct. 9, 404–416.

López-Realpozo, J.C., Rodríguez-Ramos, R., Guinovart-Díaz, R., Bravo-Castillero, J., Sabina, F.J., 2011. Transport properties in fibrous elastic rhombic composite with imperfect contact condition. Int. J. Mech. Sci. 53, 98–107.

López-Realpozo, J.C., Rodríguez-Ramos, R., Guinovart-Díaz, R., Bravo-Castillero, J., Otero, J.A., Sabina, F.J., Lebon, F., Dumont, S., Sevostianov, I., 2014. Effective elastic shear stiffness of a periodic fibrous composite with non-uniform imperfect contact between the matrix and the fibers. Int. J. Solids Struct. 51, 1253-1262.

Mclaughlin, R., 1977. A study of the differential scheme for composite materials. Int. J. Eng. Sci. 15(4), 237–244.

Mori, T., Tanaka, K., 1973. Average stress in matrix and average elastic energy of materials with misfitting inclusions. Acta Metall. Sin. 21, 571–574.

Nan, C.W., 1994. Magnetoelectric effect in composites of piezoelectric and piezomagnetic phases. Phys. Rev. B 50, 6082–6088.

Nan, C.W., Bichurin, M.I., Dong, S., Viehland, D., Srinivasan, G., 2008. Multiferroic magnetoelectric composites: historical perspective, status and future directions. J. Appl. Phys. 103, 031101.

ACCEPTED MANUSCRIPT

Nemat-Nasser, S., Hori, M., 1999. Micromechanics: Overall Properties of Heterogeneous Materials, North-Holland, Amsterdam.

Otero, J. A., Rodríguez-Ramos, R., Monsivais, G., Stern, C., Martínez, R., Dario, R., 2014. Interfacial waves between two magneto-electro-elastic half-spaces with magneto-electro-mechanical imperfect interface. Philos. Mag. Lett. 94(10), 629–638.

Parton, V.Z., Kudryavtsev, B.A., 1993. Engineering Mechanics of Composite Materials. CRC Press, Boca Raton.

Pobedrya, B.E., 1984. Mechanics of composite materials. Moscow State University Press, in Russian.

Rodríguez-Ramos, R., Guinovart-Díaz, R., López-Realpozo, J.C., Bravo-Castillero, J., Sabina, F.J., 2010. Influence of imperfect elastic contact condition on the antiplane effective properties of piezoelectric fibrous composites. Appl. Mech. 80, 377–388.

Rodríguez-Ramos, R., Yan, P., López-Realpozo, J.C., Guinovart-Díaz, R., Bravo-Castillero J., Sabina, F.J., Jiang, C.P., 2011. Two analytical models for the study of periodic fibrous elastic composite with different unit cells. Compos. Struct. 93, 709–714.

Rodríguez-Ramos, R., de Medeiros, R., Guinovart-Díaz, R., Bravo-Castillero, J., Otero, J.A., Tita, V., 2013. Different approaches for calculating the effective elastic properties in composite materials under imperfect contact adherence. Compos. Struct. 99, 264–275.

Sevostianov, I., Rodríguez-Ramos, R., Guinovart-Díaz, R., Bravo-Castillero J., Sabina, F.J., 2012. Connections between different models describing imperfect interfaces in periodic fiber-reinforced composites. Int. J. Solids Struct. 49, 1518–1525.

ACCEPTED MANUSCRIPT

ACCEPTED MANUSCRIPT

Sixto-Camacho, L.M., Bravo-Castillero, J., Brenner, R., Guinovart-Díaz, R., Mechkuor, H., Rodríguez-Ramos, R., Sabina, F.J., 2013. Asymptotic homogenization of periodic thermo-magneto-electro-elastic heterogeneous media. Comput. Math. Appl. 66, 2056–2074.

Sixto-Camacho, L.M., Bravo-Castillero, J., Guinovart-Díaz, R., Pérez-Fernández, L.D., Rodríguez-Ramos, R., Sabina, F.J., 2015. Exact relations for the anti-plane effective magneto-electro-elastic coefficients of two-phase fibrous composites. Mech. Res. Commun. 70, 42–48.

Tong, Z.H., Lo, S.H., Jiang, C.P., Cheung, Y.K., 2008. An exact solution for the three-phase thermo-electro-magneto-elastic cylinder model and its application to piezoelectric–magnetic fiber composites. Int. J. Solids Struct. 45, 5205–5219.

Van den Boomgaard, J., Terrell, D.R., Born, R.A.J. and Giller, H.F.J.I., 1974. An in situ grown eutectic magnetoelectric composite material. Part I: composition and unidirectional solidification. J. Mater. Sci. 9(10), 1705 - 1709.

Van den Boomgaard, J., Born, R.A.J., 1978. A Sintered Magnetoelectric Composite Material $BaTiO_3$-Ni(Co, Mn)Fe_3O_4. J. Mater. Sci. 13, 1538-1548.

Van Suchtelen, J., 1972. Product properties: a new application of composite materials. Philips Res. Rep. 27, 28–37.

Van Run, A.M.J.G., Terrell, D.R., Scholing, J.H., 1974. An in situ grown eutectic magnetoelectric composite materials. Part 2: physical properties. J. Mater. Sci. 9, 1710–1714.

Wang, J., Duan, H.L., Zhang, Z., Huang Z.P., 2005. An anti-interpenetration model and connections between interphase and interface models in particle-reinforced composites. Int. J. Mech. Sci. 47, 701–718.

Wang, H.M., Ding, H.J., 2006. Transient responses of a magneto-electro-elastic hollow sphere for fully coupled spherically symmetric problem. Eur. J. Mech. A. Solids 25, 965–980.

ACCEPTED MANUSCRIPT

Wang, X., Pan, E., 2007. Magnetoelectric effects in multiferroic fibrous composite with imperfect interface. Phys. Rev. B 76, 214107.

Wang, Y., Su Y., Li J., Weng G.J., 2015. A theory of magnetoelectric coupling with interface effects and aspect-ratio dependence in piezoelectric-piezomagnetic composites. J. Appl. Phys. 117, 164106.

Wang, Y.Z., 2015. Influences of imperfect interface on effective magnetoelectric properties in multiferroic composites with elliptical fibers. Smart Mater. Struct. 24, 045021.

Wu, T.L. and Huang, J.H., 2000. Closed-form solutions for the magnetoelectric coupling coefficients in fibrous composites with piezoelectric and piezomagnetic phases. Int. J. Solids Struct. 37, 2981–3009.

Wüerkner, M., Berger, H. and Gabbert, U., 2013. Numerical study of effective elastic properties of fiber reinforced composites with rhombic cell arrangements and imperfect interface. Int. J. Eng. Sci. 63, 1–9.

Xu, Y.L. and Xiao, J.H., 2015. An analytical method for predicting the anti-plane effective magnetoelectroelastic coefficients of composites containing doubly periodic multicoated fibers. Z. angew. Math. Mech. 1–14. doi: 10.1002/zamm.201500003.

Yan, P., Jiang, C.P., Song, F., 2013. Unified series solution for the anti-plane effective magnetoelectroelastic moduli of three-phase fiber composites. Int. J. Solids Struct. 50, 176–185.

ACCEPTED MANUSCRIPT

Table captions

Table 1. Local problems with associated local functions.

Local Problem	**X**	**Y**	**Z**	Φ_1	Φ_2	Φ_3
${}_{13}\mathcal{L}\,({}_{23}\mathcal{L})$	${}_{13}\tilde{\mathrm{L}}_3\,({}_{23}\tilde{\mathrm{L}}_3)$	${}_{13}\tilde{\mathrm{M}}\,({}_{23}\tilde{\mathrm{M}})$	${}_{13}\tilde{\mathrm{N}}\,({}_{23}\tilde{\mathrm{N}})$	$C^{(\gamma)}_{1313}$	$e^{(\gamma)}_{113}$	$q^{(\gamma)}_{113}$
${}_{1}\mathcal{I}\,({}_{2}\mathcal{I})$	${}_{1}\tilde{\mathrm{P}}_3\,({}_{2}\tilde{\mathrm{P}}_3)$	${}_{1}\tilde{\mathrm{Q}}\,({}_{2}\tilde{\mathrm{Q}})$	${}_{1}\tilde{\mathrm{R}}\,({}_{2}\tilde{\mathrm{R}})$	$e^{(\gamma)}_{131}$	$-\kappa^{(\gamma)}_{11}$	$-\alpha^{(\gamma)}_{11}$
${}_{1}\mathcal{P}\,({}_{2}\mathcal{P})$	${}_{1}\tilde{\mathrm{S}}_3\,({}_{2}\tilde{\mathrm{S}}_3)$	${}_{1}\tilde{\mathrm{T}}\,({}_{2}\tilde{\mathrm{T}})$	${}_{1}\tilde{\mathrm{V}}\,({}_{2}\tilde{\mathrm{V}})$	$q^{(\gamma)}_{131}$	$-\alpha^{(\gamma)}_{11}$	$-\mu^{(\gamma)}_{11}$

Table 2. Local Problems and the corresponding independent terms.

Local Problem	T_1	T_2	T_3	Local Problem	T_1	T_2	T_3
${}_{13}\mathcal{L}$	$\mathcal{A}_{2p}$	$\mathcal{A}_{4p}$	$\mathcal{A}_{6p}$	${}_{23}\mathcal{L}$	$\mathcal{A}_{2p}$	$\mathcal{A}_{4p}$	$\mathcal{A}_{6p}$
${}_{1}\mathcal{I}$	$\mathcal{B}_{2p}$	$\mathcal{B}_{4p}$	$\mathcal{B}_{6p}$	${}_{2}\mathcal{I}$	$\mathcal{B}_{2p}$	$\mathcal{B}_{4p}$	$\mathcal{B}_{6p}$
${}_{1}\mathcal{P}$	$\mathcal{C}_{2p}$	$\mathcal{C}_{4p}$	$\mathcal{C}_{6p}$	${}_{2}\mathcal{P}$	$\mathcal{C}_{2p}$	$\mathcal{C}_{4p}$	$\mathcal{C}_{6p}$

Table 3. Material properties used in the numerical simulations.

Material Properties	$C^{(\gamma)}_{55}$ (N/m^2)	$e^{(\gamma)}_{15}$ (C/m^2)	$\kappa^{(\gamma)}_{11}$ (C^2/Nm^2)	$q^{(\gamma)}_{15}$ (N/Am)	$\alpha^{(\gamma)}_{11}$ (Ns/VC)	$\mu^{(\gamma)}_{11}$ (Ns^2/C^2)
$BaTiO_3$ (BTO)	43 x 10^9	11.6	11.2 x 10^{-9}	0	0	5 x 10^{-6}
$CoFe_2O_4$ (CFO)	45.3 x 10^9	0	0.08 x 10^{-9}	550	0	590 x 10^{-6}
Terfenol-D (TD)	13.6 x 10^9	0	0.05 x 10^{-9}	108.3	0	5.4 x 10^{-6}

Table 4. A comparison of MEE effective coefficients obtained by the present model (AHM) for a two-phase composite BTO/CFO with the models reported by Yan et al. (2013), Kuo (2011), Espinosa-Almeyda et al. (2014) (AHM three-phase model), and Xu and Xiao (2015).

Composite: fiber/matrix = BTO/CFO									
N_0	C^*_{1313} (GPa)			e^*_{113} (C/m^2)			κ^*_{11} (10^{-9} C^2/ Nm^2)		
	Present model	Yan et al., 2013	AHM three-phase model	Present model	Yan et al., 2013	AHM three-phase model	Present model	Yan et al., 2013	AHM three-phase model
1	50.79	50.78	50.79	0.2579	0.2768	0. 2579	0.3362	0.3544	0.3362
3	50.79	50.79	50.79	0.2588	0.2596	0.2588	0.3371	0.3379	0.3371
5	50.79	50.79	50.79	0.2588	0.2587	0.2588	0.3371	0.337	0.3371
7	50.79	50.79	50.79	0.2588	0.2588	0.2588	0.3371	0.3371	0.3371
9	50.79	50.79	50.79	0.2588	0.2588	0.2588	0.3371	0.3371	0.3371
Kuo	50.8			0.255			0.337		

ACCEPTED MANUSCRIPT

Xu-Xiao	50.792			0.25822			0.33654		
N_0	q_{15}^* (N/Am)			μ_{11}^* (10^{-6} Ns^2/C^2)			$-\alpha_{11}^*$ (10^{-12} Ns/VC)		
	Present model	Yan et al. 2013	AHM three-phase model	Present model	Yan et al., 2013	AHM three-phase model	Present model	Yan et al., 2013	AHM three-phase model
1	128.4	163.4	128.4	141.4	178.7	141.4	6.017	5.562	6.018
3	128.0	130.7	128.0	141.0	143.8	141.0	6.020	5.987	6.020
5	128.0	128.1	128.0	141.0	141.1	141.0	6.020	6.019	6.020
7	128.0	128.0	128.0	141.0	141.0	141.0	6.020	6.020	6.020
9	128.0	128.0	128.0	141.0	141.0	141.0	6.020	6.020	6.020
Kuo	128			140			6.03		
Xu-Xiao	128.23			141.24			6.0181		

Table 5. Effective properties of a two-phase MEE composite (BTO/CFO) with parallelogram-like fiber distribution under perfect contact conditions and $V_2 = 0.6$.

θ_1	C_{1313}^*	C_{1323}^*	C_{2323}^*	e_{113}^*	e_{123}^*	e_{223}^*	q_{113}^*	q_{123}^*	q_{223}^*
	(GPa)			(C/m^2)			(N/Am)		
45°	50. 807	0.1024	50. 602	0.22294	-0.12563	0.47421	86.15	-35.438	157.026
50°	50. 814	0.0343	50. 756	0.21726	-0.05093	0.30273	115.969	-19.543	148.766
60°	50. 806	0	50. 806	0.23471	0	0.23471	137.619	0	137.619
70°	50. 797	-0.0104	50. 804	0.24936	0.01902	0.23551	137.74	7.831	132.039
75°	50. 794	-0.011	50. 8	0.25386	0.02015	0.24307	134.621	8.007	130.33
80°	50. 792	-0.009	50. 796	0.25673	0.0165	0.25091	131.322	6.348	129.083
90°	50.791	0	50. 791	0.25878	0	0.25878	128.026	0	128.026
θ_1	κ_{11}^*	κ_{12}^*	κ_{22}^*	$-\alpha_{11}^*$	$-\alpha_{12}^*$	$-\alpha_{22}^*$	μ_{11}^*	μ_{12}^*	μ_{22}^*
	(nF/m)			$\times 10^{-12}$ (Ns/VC)			$\times 10^{-6}$ (Ns^2/C^2)		
45°	0.3027	-0.1204	0.5434	6.5716	0.5343	5.5029	96.409	-37.752	171.914
50°	0.2973	-0.0488	0.3792	6.1995	0.2809	5.7282	128.174	-20.819	163.113
60°	0.3140	0	0.3140	5.9151	0	5.9151	151.237	0	151.237
70°	0.3281	0.0182	0.3148	5.9039	-0.1112	5.9849	151.366	8.343	145.293
75°	0.3324	0.0193	0.3220	5.9403	-0.1142	6.0014	148.044	8.531	143.472
80°	0.3351	0.0158	0.3295	5.9800	-0.0908	6.0121	144.53	6.762	142.145
90°	0.3371	0	0.3371	6.0203	0	6.0203	141.019	0	141.019

Table 6. Variations of the ME coefficients α_{11}^*, α_{12}^* and α_{22}^* for a CFO/BTO composite for three types RVEs and different imperfections values of K, M and N.

Magnetoelectric coefficients $(-\alpha_{11}^*, -\alpha_{12}^*, -\alpha_{22}^*)$ $\times 10^{-12}$ (Ns/VC)			
$V_2 = 0.6$	60°	90°	75°

			$-\alpha_{11}^*$		$-\alpha_{11}^*$	$-\alpha_{11}^*$	$-\alpha_{12}^*$	$-\alpha_{22}^*$
K	M	N	Present model	Wang and Pan (2007)	Present model	Present model		
0	0	0	5.26117	5.26117	5.40018	5.30002	-0.12993	5.36965
1	0	0	2.86437	2.86437	3.51417	3.18576	-0.04218	3.20836
10	0	0	0.56159	0.56159	0.75394	0.66091	-0.00216	0.66207
0	1	0	2.63248	2.6325	2.69568	2.64854	-0.06564	2.68372
0	10	0	0.47887	0.47887	0.49007	0.48163	-0.012	0.48806
0	0	10	3.96204	3.96204	4.07019	3.96465	-0.19456	4.06892
0	0	250	0.57199	0.57199	0.6791	0.61419	-0.05754	0.64503
K=M=N=10 (only AHM)			0.03844		0.04603	0.04189	-0.00187	0.04289

Table 7. MEE effective properties for BTO/CFO composite with parallelogram-like RVE and fiber volume fraction $V_2 = 0.6$ and $N_0 = 9$.

θ_1 = 45°			C_{1313}^*	C_{2313}^*	C_{2323}^*	e_{113}^*	e_{213}^*	e_{223}^*	q_{113}^*	q_{213}^*	q_{213}^*
K	M	N	(GPa)			(C/m^2)			(N/Am)		
0	0	0	50.807	0.1024	50.602	0.2229	-0.1256	0.4742	86.150	-35.438	157.026
10	0	0	11.637	-2.312	16.261	0.0219	-0.0092	0.0402	84.063	-36.069	156.202
0	10	0	50.859	0.028	50.803	0.1628	-0.0498	0.2623	86.151	-35.438	157.027
0	0	10	50.808	0.1028	50.603	0.2229	-0.1256	0.4742	83.935	-36.121	156.176
10	10	10	11.637	-2.312	16.262	0.0163	-0.0030	0.0224	83.772	-36.168	156.109
θ_1 = 75°			C_{1313}^*	C_{2313}^*	C_{2323}^*	e_{113}^*	e_{213}^*	e_{223}^*	q_{113}^*	q_{213}^*	q_{213}^*
K	M	N	(GPa)			(C/m^2)			(N/Am)		
0	0	0	50.794	-0.011	50.8	0.2539	0.0201	0.2431	134.62	8.0074	130.33
10	0	0	14.745	0.5356	14.458	0.0235	0.0014	0.0227	133.56	8.0926	129.23
0	10	0	50.847	-0.0030	50.848	0.1907	0.0115	0.1846	134.62	8.0075	130.33
0	0	10	50.794	-0.011	50.80	0.2539	0.0201	0.2431	133.54	8.0908	129.207
10	10	10	14.745	0.5356	14.458	0.0176	0.0007	0.0173	133.45	8.0998	129.113
θ_1 = 45°			κ_{11}^*	κ_{12}^*	κ_{22}^*	$-\alpha_{11}^*$	$-\alpha_{12}^*$	$-\alpha_{22}^*$	μ_{11}^*	μ_{12}^*	μ_{22}^*
K	M	N	x 10^{-9} (C^2/Nm^2)			x 10^{-12} (Ns/VC)			x 10^{-6} (Ns^2/C^2)		
0	0	0	0.3027	-0.1204	0.5434	6.5716	0.5343	5.5029	96.409	-37.752	171.914
10	0	0	0.3044	-0.1230	0.5505	0.9536	0.1207	0.7122	96.41	-37.752	171.914
0	10	0	0.2315	-0.0436	0.3187	5.427	0.8461	3.7348	96.409	-37.752	171.914
0	0	10	0.3027	-0.1204	0.5434	0.6014	0.0501	0.5012	90.405	-38.723	167.85
10	10	10	0.2322	-0.0442	0.3206	0.0616	0.0124	0.0368	90.405	-38.723	167.85
θ_1 = 75°			κ_{11}^*	κ_{12}^*	κ_{22}^*	$-\alpha_{11}^*$	$-\alpha_{12}^*$	$-\alpha_{22}^*$	μ_{11}^*	μ_{12}^*	μ_{22}^*
K	M	N	x 10^{-9} (C^2/Nm^2)			x 10^{-12} (Ns/VC)			x 10^{-6} (Ns^2/C^2)		
0	0	0	0.3324	0.0193	0.3220	5.9403	-0.1142	6.0015	148.04	8.5307	143.472
10	0	0	0.334	0.0196	0.3235	0.6557	-0.0062	0.6590	148.04	8.5307	143.472

0	10	0	0.256	0.01	0.2507	4.5960	-0.1914	4.6986	148.04	8.5307	143.472
0	0	10	0.3324	0.0193	0.3220	0.5417	-0.0104	0.5473	143.59	8.6739	138.939
10	10	10	0.2569	0.0102	0.2515	0.0429	-0.0019	0.0439	143.59	8.6739	138.939

Table 8. Effect of imperfect parameters in the overall magneto-electro-elastic properties of composites.

Imperfect parameters	Composite: BTO/CFO	
	affected	not affected
K	C^*_{1313}, C^*_{2313}, C^*_{2323}, e^*_{113}, e^*_{213}, e^*_{223}, α^*_{11}, α^*_{12}, α^*_{22}.	q^*_{113}, q^*_{213}, q^*_{223}, κ^*_{11}, κ^*_{12}, κ^*_{22}, μ^*_{11}, μ^*_{12}, μ^*_{22}.
M	C^*_{2313}, e^*_{113}, e^*_{213}, e^*_{223}, κ^*_{11}, κ^*_{12}, κ^*_{22}, α^*_{11}, α^*_{12}, α^*_{22}.	C^*_{1313}, C^*_{2323}, q^*_{113}, q^*_{213}, q^*_{223}, μ^*_{11}, μ^*_{12}, μ^*_{22}.
N	α^*_{11}, α^*_{12}, α^*_{22}.	C^*_{1313}, C^*_{2313}, C^*_{2323}, e^*_{113}, e^*_{213}, e^*_{223}, q^*_{113}, q^*_{213}, q^*_{223}, κ^*_{11}, κ^*_{12}, κ^*_{22}, μ^*_{11}, μ^*_{12}, μ^*_{22}.
Imperfect parameters	Composite: CFO/BTO	
	affected	not affected
K	C^*_{1313}, C^*_{2313}, C^*_{2323}, q^*_{113}, q^*_{213}, q^*_{223}, α^*_{11}, α^*_{12}, α^*_{22}.	e^*_{113}, e^*_{213}, e^*_{223}, κ^*_{11}, κ^*_{12}, κ^*_{22}, μ^*_{11}, μ^*_{12}, μ^*_{22}.
M	α^*_{11}, α^*_{12}, α^*_{22}.	C^*_{1313}, C^*_{2313}, C^*_{2323}, e^*_{113}, e^*_{213}, e^*_{223}, q^*_{113}, q^*_{213}, q^*_{223}, κ^*_{11}, κ^*_{12}, κ^*_{22}, μ^*_{11}, μ^*_{12}, μ^*_{22}.
N	q^*_{113}, q^*_{213}, q^*_{223}, α^*_{11}, α^*_{12}, α^*_{22}, μ^*_{11}, μ^*_{12}, μ^*_{22}.	C^*_{1313}, C^*_{2313}, C^*_{2323}, e^*_{113}, e^*_{213}, e^*_{223}, κ^*_{11}, κ^*_{12}, κ^*_{22}.

Figure captions

ACCEPTED MANUSCRIPT

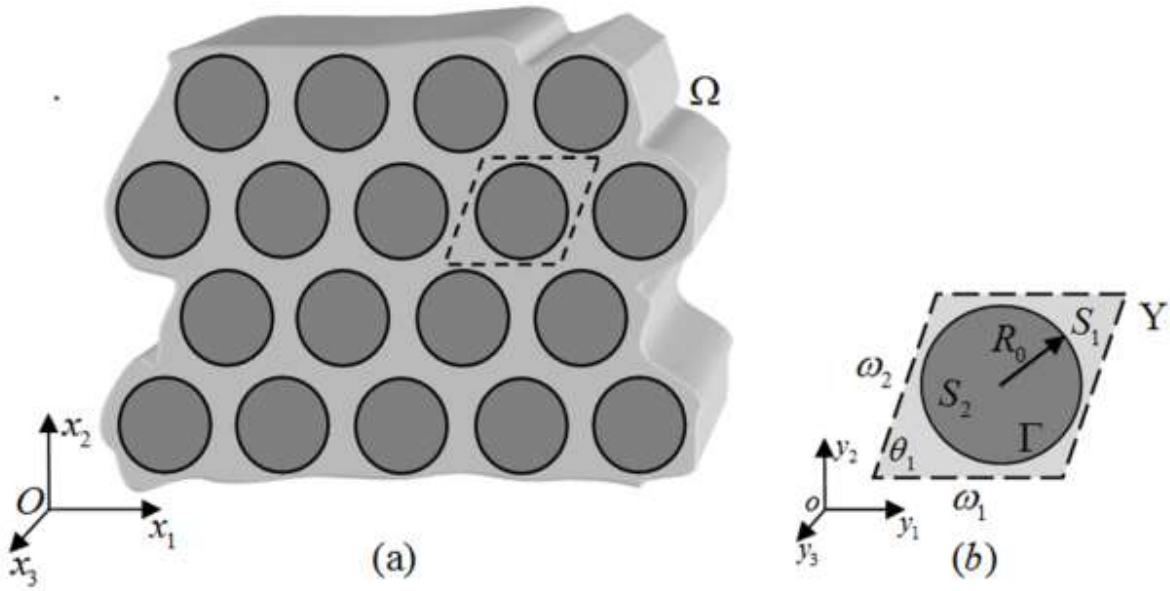

Fig. 1. (a) Representative cross section of a two-phase MEE fiber composite with a doubly periodic microstructure and (b) extracted parallelogram RVE.

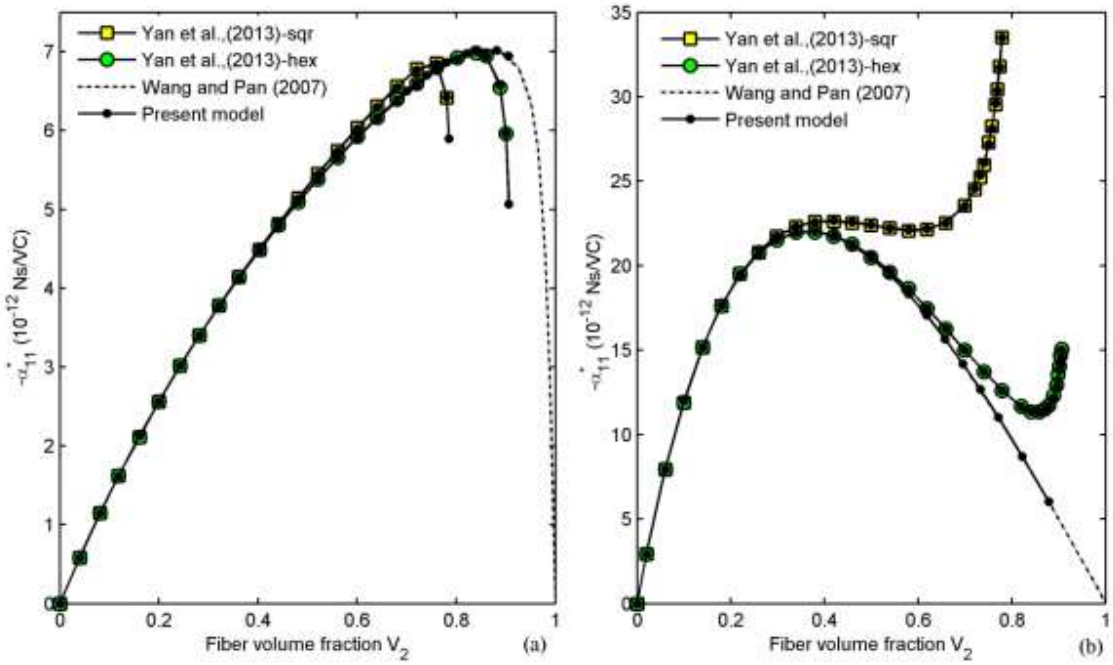

Fig. 2. Variation of the effective ME coefficients $(\alpha_{11}^{*} = \alpha_{22}^{*})$ versus the fiber volume fraction V_2. Comparison with Wang and Pan (2007) and Yan et al., (2013) models for a two-phase composite with square or hexagonal RVE under perfect contact condition is reported. (a) CFO/BTO; (b) TD/BTO.

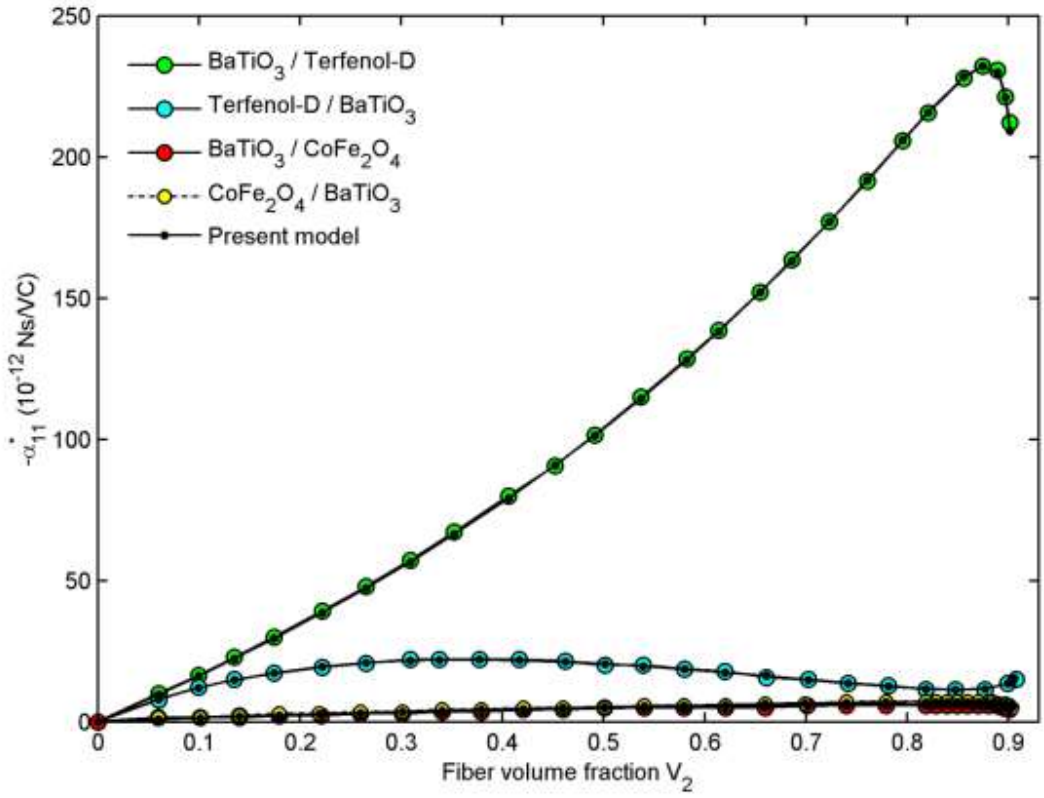

Fig. 3. Variation of the effective ME coefficients $(\alpha_{11}^{*} = \alpha_{22}^{*})$ versus the fiber volume fraction V_2. Comparisons between the AHM (present model) and Yan et al., (2013) models for different two-phase composites considering hexagonal RVE under perfect contact conditions.

ACCEPTED

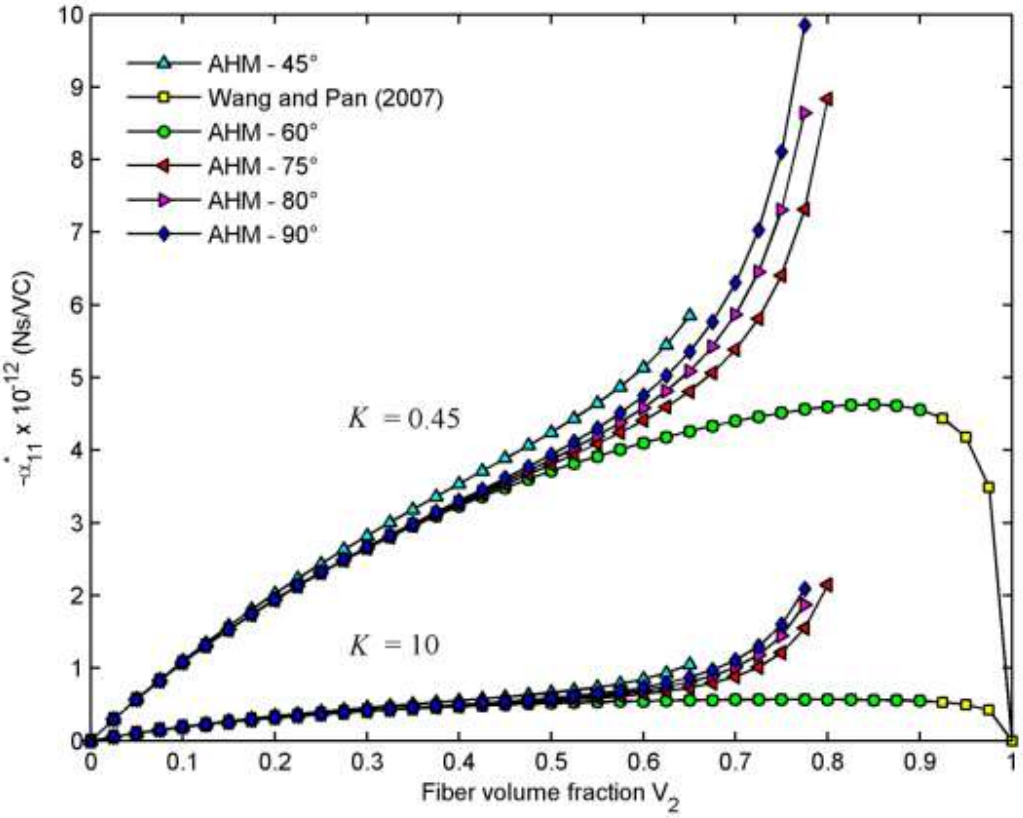

Fig. 4. Variation of the effective ME coefficient α_{11}^{*} of a two-phase MEE composite (BTO/CFO) versus the fiber volume fraction V_2 for different parallelogram-like RVEs under two kind of mechanical imperfections.

ACCEPTED MANUSCRIPT

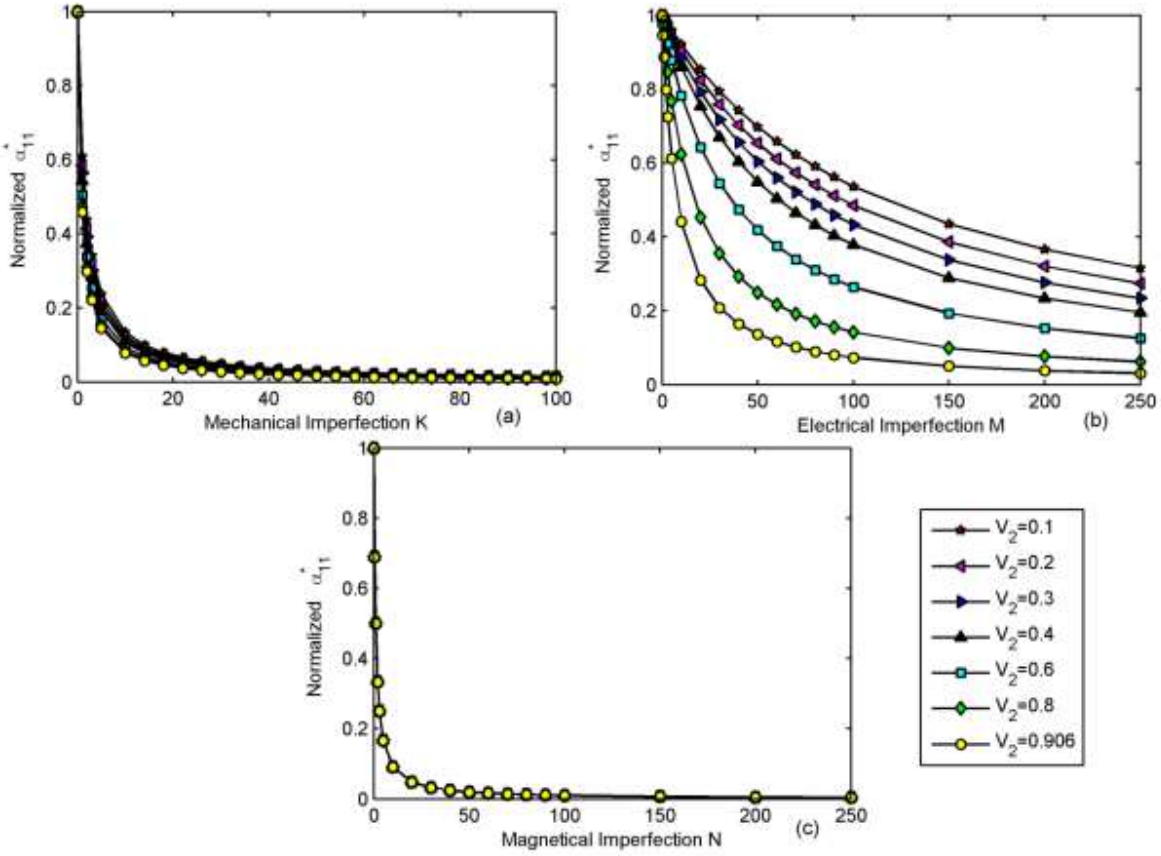

Fig. 5. Variation of the normalized ME effective coefficient α_{11}^* versus the interfacial imperfections for different fiber volume fractions of $BaTiO_3$.

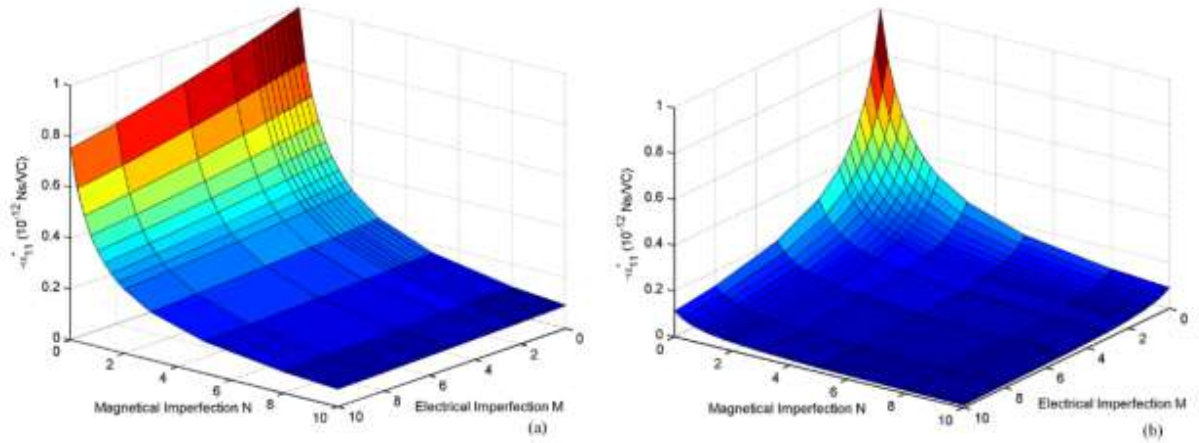

Fig. 6. Variation of the normalized ME effective coefficient α_{11}^{*} under electrical and magnetical imperfections for a two-phase composite with hexagonal RVE. (a) CFO/BTO; (b) TD/BTO.

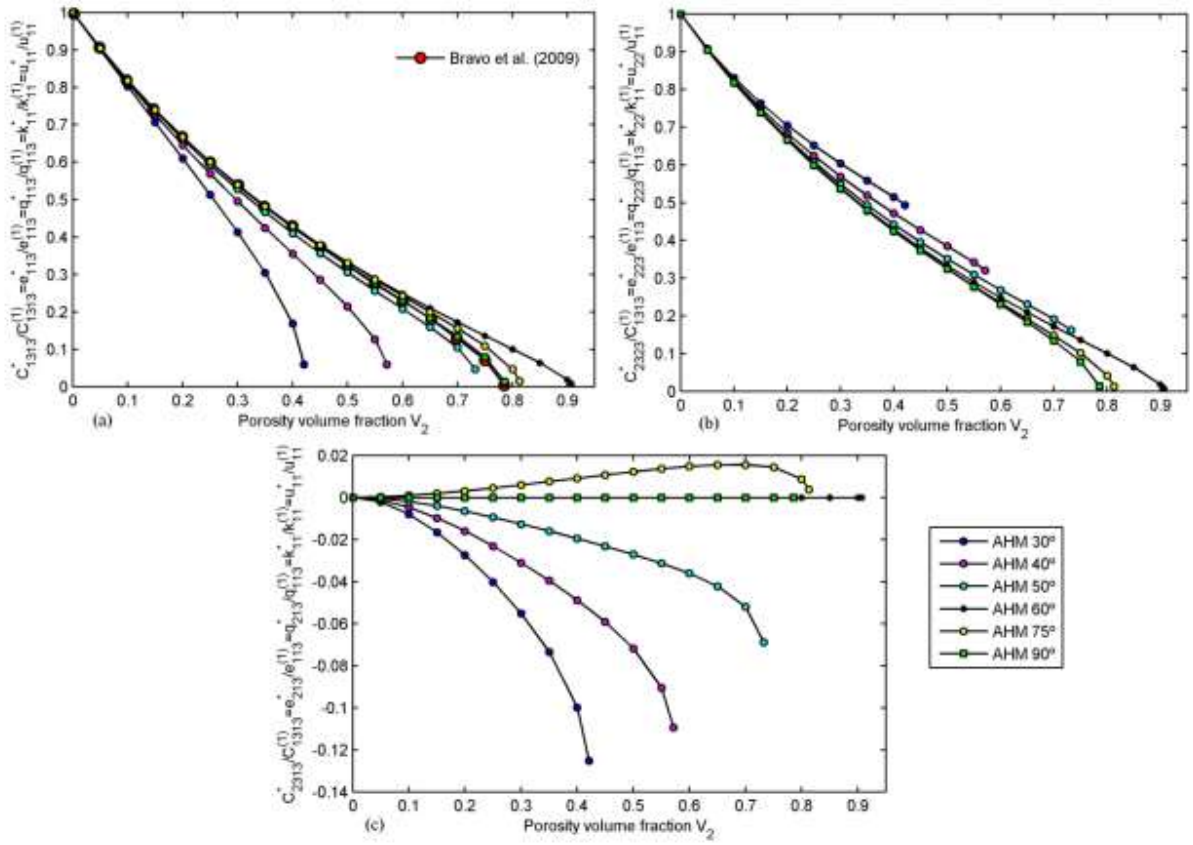

Fig. 7. The normalized effective properties of the two-phase composite with empty fiber versus the volume fraction of the fiber for different fiber array.

ACCEPTED